An Accurate Power-Sharing Control Method Based on Circulating-Current Power Phasor Model in Voltage-Source Inverter Parallel-Operation System

Mingzhi Gao, *Member, IEEE*, Min Chen, *Member, IEEE*, Chenxi Wang, and Zhaoming Qian, *Senior Member, IEEE*

***Abstract*—This paper proposes an optimized mathematical model of the voltage-source inverter parallel-operation system (VSIPS) and proposes an improved droop control method based on this model, which can realize accurate power sharing in VSIPS. First, this paper analyzes VSIPS as a multi-input and multioutput system and proposes a precise definition of circulating current. The circulating-current model, the steady-state model, and the small-signal model are proposed subsequently based on the optimum design of wire impedance, which constitute the optimized mathematical model of VSIPS in *s*-domain. The circulating-current phasor model and the circulating-current power phasor model (CCPPM) are also proposed. Second, the mathematical model of traditional droop control is built and analyzed based on CCPPM, which elaborates the tradeoff of droop control between the steady-state voltage bias and the load-sharing accuracy, and proves that the $V-Q$ droop control cannot realize accurate reactive-power sharing. Third, an improved droop control method ($\omega-P_{\rm cir}$ and $V-Q_{\rm cir}$ control) is proposed, which can realize the accurate active- and reactive-power sharing and eliminate the steady-state voltage bias simultaneously. Finally, simulation and experimental results are presented, which validate the proposed mathematical model of VSIPS, the analysis of droop control, and the performance of the proposed method.**

***Index Terms*—Inverters, power control, power system modeling, system analysis and design.**

NOMENCLATURE

A	Common factor defined in (14).
a	Serial number of any VSI in VSIPS.
CSI	Current-source inverter.
CCPPM	Circulating-current power phasor model.
ϕ_e	Phase of Z_e in phasor model.
$\phi_{w.a}$	Phase of $Z_{w.a}$ in phasor model.
$I_{\rm cir}$	Circulating current.
$I_{{\rm cir}.a}$	Circulating current of any VSI.
$I_{{\rm cir}.a.{\rm RMS}}$	Effective value of $I_{{\rm cir}.a}$.
$I_{{\rm cir}.a.p}$	Real component of $I_{{\rm cir}.a}$ in phasor model.
$I_{{\rm cir}.a.q}$	Imaginary component of $I_{{\rm cir}.a}$ in phasor model.
$I_{\rm cir.RMS}$	Equivalent circulating current of VSIPS.
$I_{\rm load}$	Current of the common load.
$I_{o.a}$	Actual output current of any VSI.
$I_{t.a}$	Theoretical output current of any VSI.
k	Serial number of control cycle.
k_a	Weight coefficient of any VSI in load sharing.
L_e	Inductance of Z_e.
$L_{w.a}$	Inductance of $Z_{w.a}$.
$m_{T.a}$	Optimum value of $m_{\omega.a}$ in $\omega-P_{\rm cir}$ control.
$m_{T.e}$	Optimum value of $m_{\omega.e}$ in $\omega-P_{\rm cir}$ control.
$m_{\omega.a}$	$\omega-P$ and $\omega-P_{\rm cir}$ droop coefficient of any VSI.
$m_{\omega.e}$	$\omega-P$ and $\omega-P_{\rm cir}$ equivalent droop coefficient.
n	Total number of VSIs in VSIPS.
$n_{T.a}$	Optimum value of $n_{v.a}$ in $V-Q_{\rm cir}$ control.
$n_{T.e}$	Optimum value of $n_{v.e}$ in $V-Q_{\rm cir}$ control.
$n_{v.a}$	$V-Q$ and $V-Q_{\rm cir}$ droop coefficient of any VSI.
$n_{v.e}$	$V-Q$ and $V-Q_{\rm cir}$ equivalent droop coefficient.
$P_{\rm cir}$	Active circulating-current power (CCP).
$P_{{\rm cir}.a}$	Active CCP of any VSI.
$P_{{\rm cir}.a.k}$	$P_{{\rm cir}.a}$ in the kth control cycle.
$P_{\rm cir.RMS}$	Equivalent active CCP of VSIPS.
$P_{o.a}$	Active output power of any VSI.
$P_{o.a.k}$	$P_{o.a}$ in the kth control cycle.
$P_{\rm to}$	Active output power of VSIPS.
$Q_{\rm cir}$	Reactive CCP.
$Q_{{\rm cir}.a}$	Reactive CCP of any VSI.
$Q_{{\rm cir}.a.k}$	$Q_{{\rm cir}.a}$ in the kth control cycle.
$Q_{\rm cir.RMS}$	Equivalent reactive CCP of VSIPS.
$Q_{o.a}$	Reactive output power of any VSI.
$Q_{o.a.k}$	$Q_{o.a}$ in the kth control cycle.
$Q_{\rm to}$	Reactive output power of VSIPS.
θ_a	Phase difference between V_m and $V_{o.a}$ in phasor model.
$\theta_{a.0}$	Value of θ_a in the initial control cycle.
$\theta_{a.k}$	Value of θ_a in the kth control cycle.
$\theta_{d.0}$	Phase of $V_{m.d.0}$.
$\theta_{d.k}$	Phase of $V_{m.d.k}$.
R_e	Resistance of Z_e.
$R_{w.a}$	Resistance of $Z_{w.a}$.
S_1, S_2, S_3	Polynomials defined in (57).

Manuscript received May 6, 2017; accepted June 9, 2017. Date of publication June 27, 2017; date of current version February 1, 2018. This work was supported by the China National Science Fund under Grant 51477153. Recommended for publication by Associate Editor J. M. Guerrero. *(Corresponding author: Min Chen.)*

The authors are with the Department of Applied Electronics, Zhejiang University, Hangzhou 310057, China (e-mail: xiaosan433@zju.edu.cn; calim@zju.edu.cn; zjushine@zju.edu.cn; qian@zju.edu.cn).

Color versions of one or more of the figures in this paper are available online at http://ieeexplore.ieee.org.

Digital Object Identifier 10.1109/TPEL.2017.2720479

$S_{\text{cir}.a}$	Circulating-current complex power of any VSI.
$S_{o.a}$	Complex output power of any VSI.
$S_{\text{RA}.a}$	Rated output power of any VSI.
S_{TA}	Total rated output power of VSIPS.
S_{to}	Complex output power of VSIPS.
$T_{c.\omega}$	Time of $\omega - P$ and $\omega - P_{\text{cir}}$ control cycle.
U_{bus}	Voltage of ac bus (Equals U_{load}).
U_{load}	Voltage of Z_{load} (Equals U_{bus}).
V^*	Rated effective value of all VSIs' voltages.
V_A	Effective value of V_m.
$V_{A.d}$	Value of $V_{A.d.k}$ in the steady state.
$V_{A.d.0}$	Effective value of $V_{m.d.0}$.
$V_{A.d.k}$	Effective value of $V_{m.d.k}$.
$V_{a.0}$	Effective value of $V_{o.a}$ in the initial control cycle.
$V_{a.k}$	Effective value of $V_{o.a}$ in the kth control cycle.
V_m	Weighted average of all VSIs' output voltages.
$V_{m.d.0}$	V_m in the initial control cycle in droop control.
$V_{m.d.k}$	V_m in the kth control cycle in droop control.
$V_{o.a}$	Output voltage of any VSI.
$\Delta V_{o.a}$	Difference of $V_{o.a}$ and V_m.
$V_{\text{ref}.a}$	Reference voltage of any VSI.
$V_{\text{rms}.a}$	Effective value of $V_{o.a}$.
VSI	Voltage-source inverter.
VSIPS	Voltage-source inverter parallel-operation system.
ω	Angel frequency of V_m.
ω^*	Rated angular frequency of all VSIs' voltages.
$\omega_{a.0}$	Angular frequency of $V_{o.a}$ in the initial control cycle.
$\omega_{a.k}$	Angular frequency of $V_{o.a}$ in the kth control cycle.
ω_d	Value of $\omega_{d.k}$ in the steady state.
$\omega_{d.0}$	Angular frequency of $V_{m.d.0}$.
$\omega_{d.k}$	Angular frequency of $V_{m.d.k}$.
Z_d	Equivalent load at the rated output power of VSIPS.
Z_E	Amplitude of Z_e in phasor model.
Z_e	Equivalent wire impedance of VSIPS.
Z_{load}	Common load of VSIPS.
$Z_{\text{rms}.a}$	Amplitude of $Z_{w.a}$ in phasor model.
Z_w	Wire impedance between VSIs and ac bus.
$Z_{w.a}$	Wire impedance between any VSI and ac bus.

I. Introduction

DROOP control is a classical control strategy of VSIPS, which is used to realize the power sharing among the VSIs. The advantages of droop control are the excellent reliability and expansibility since the communication can be avoided [1]. However, there is a natural steady-state frequency and amplitude bias of VSIs' voltage in droop control, which is influenced simultaneously by droop coefficients and the load power. Meanwhile, the steady-state voltage bias comes into conflict with the load-sharing accuracy, which is well known as the tradeoff of droop control [2].

In attempts to solve this problem, many improved droop control strategies were proposed in [2]–[35], which can obtain better static or dynamic power-sharing performance. In these references, some strategies do not need the communication, and they are proposed based on the design of virtual output impedance [2]–[7], the decoupling of output current and output power [8]–[10], the compensation of complex wire impedance [11]–[14], the analysis and improvement of power calculation methods [15], [16], the compensation of harmonic power [17], the adaptive control [18]–[20], or the design of combined droop control [21]–[24]. Meanwhile, the other proposed strategies were designed by introducing the communication among VSI modules, which can change the control structure of droop method and realize more complicated control strategies, such as the master–slave control [25], [26], the centralized control [27], [28], the distributed control [29], [30], and the hierarchical control [31]–[35].

Traditional droop control is usually analyzed based on an identical theoretical model, which can be presented in [3] and [4]. In this model, the ac bus and VSI are equivalent to the ideal voltage sources, and every VSI is conceived as a separate system. Therefore, only the output power flow between the single VSI and the ac bus is analyzed, but the relationships among VSIs are ignored. Furthermore, this model does not present the accurate definition of circulating current, especially for VSIPS in which the load is shared by more than two VSIs with different ratios. Therefore, the accurate mathematical model of circulating current and the circulating-current-eliminating mechanism are not clear in this model.

In fact, VSIPS is a multi-input and multioutput system, which needs to be analyzed as an organic whole. System inputs are the voltages of VSIs, and system outputs can be defined as output currents or circulating currents of VSIs. Distributed load of users is an unascertainable and uncontrollable variable, and the ac bus voltage is a state variable of VSIPS, influenced by VSI voltages and the user load.

Moreover, there are many factors in VSIPS, due to which the deviation will cause the difference between VSIs' output voltages, such as the components of wire impedance, the internal impedance of VSIs, the accuracy and speed of power calculation, and the control accuracy of output voltage. In order to simplify the model building and the analysis of VSIPS, every VSI module is regarded as an independent ideal voltage source, and the influence of all these factors is equivalent to the voltage difference between VSIs, including the difference between dc components and the difference between the frequency, amplitude, and phase of the fundamental and every harmonic component. Meanwhile, the purpose of the parallel-operation control strategy is to eliminate the voltage difference between the VSIs and realize the accurate power sharing of VSIs.

Based on the above-mentioned assumptions, this paper proposes the mathematical model of VSIPS in s-domain and proposes an improved droop control method based on the proposed mathematical model of CCP, which can realize the accurate power sharing in VSIPS. The major work of this paper includes three parts given as follows.

1) System Modeling and Analysis of VSIPS: This paper analyzes VSIPS as a multi-input and multioutput system and proposes a precise definition of circulating current in the VSIPS when VSIs share the power with different ratios. Subsequently,

the circulating-current model, the steady-state model, and the small-signal model are proposed based on the optimum design of wire impedance, which constitutes the proposed optimized mathematical model of VSIPS in *s*-domain. Furthermore, the circulating-current phasor model and the CCPPM are proposed based on the optimized models, which are applied to analyze the fundamental and harmonic components of the circulating current.

2) Modeling Analysis of Traditional Droop Control: On the basis of the proposed optimized mathematical model of VSIPS, this paper builds and analyzes the mathematical model of the traditional droop control based on CCPPM, which elaborates the tradeoff of droop control between the steady-state voltage bias and the load-sharing accuracy, and proves that $\omega - P$ droop control can realize accurate active-power sharing whereas $V - Q$ droop control cannot realize accurate reactive-power sharing.

3) Design of the Accurate Power Sharing Control Method: According to the analysis of droop control, this paper proposes an improved control method ($\omega - P_{\text{cir}}$ and $V - Q_{\text{cir}}$ control), which can realize the accurate active- and reactive-power sharing and eliminate the steady-state voltage bias simultaneously. The mathematical model of the proposed method is also built and analyzed.

Subsequently, the proposed mathematical model of VSIPS is verified by the simulation results on PLECS. The detailed contrast simulation and the experimental results of the traditional droop control method and the improved method are also presented, which are based on a prototype system of VSIPS (9 kVA/110 V/50 Hz) that comprises three 3-kVA VSIs. The contrast experiment comprises two parts, as the three VSIs share the load equally and unequally, and both the parts are tested in different conditions of nonload, linear load, and nonlinear load. Finally, some conclusions of this paper are given at the end of this paper.

This paper is organized as follows. Section II presents the mathematical description of VSIPS, proposes the mathematical definition of circulating current in VSIPS, and analyzes the circulating current and the steady state of VSIPS. Subsequently, the optimized mathematical model of VSIPS in *s*-domain is proposed in Section III, and the phasor model of circulating current and CCP is proposed in Section IV. In Section V, the mathematical model of traditional droop control is built and analyzed based on CCPPM. And the improved control method is proposed and analyzed by the mathematical model in Section VI. Section VII presents the simulation results of the mathematical model of VSIPS, and Section VIII presents the contrast simulation and experiment of traditional droop control method and the proposed method. Finally, the conclusions of this paper are given in Section IX.

II. System Modeling of VSIPS

A. Mathematical Description of VSIPS

Fig. 1 illustrates the equivalent diagram of VSIPS, a system which consists of *n* VSI modules [1]. In this system, each VSI

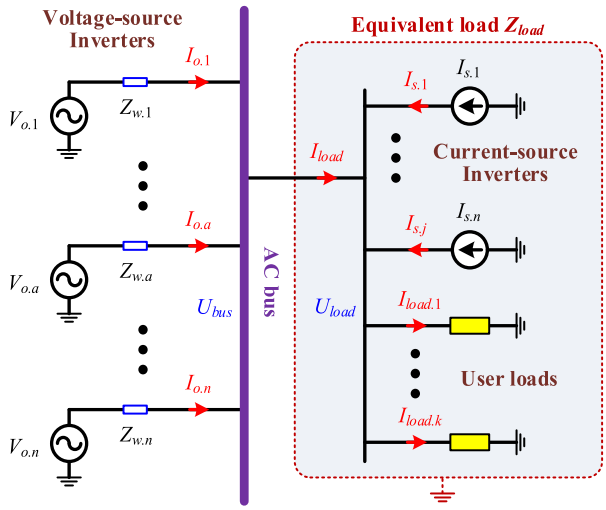

Fig. 1. Equivalent diagram of VSIPS.

module is regarded as an ideal voltage source. The influence of factors, such as the wire impedance, the internal impedance of VSIs, the accuracy and speed of power calculation, the control accuracy of output voltage, and so on, on the VSIs' voltages is equivalent to the voltage difference between VSIs, including the difference between dc components, and the difference between the frequency, amplitude, and phase of the fundamental and every harmonic component.

Meanwhile, each CSI is regarded as a special load with negative consumption power [1], [36], [37]. Therefore, all CSIs and users' loads can be equivalent to a single load (defined as the common load Z_{load}), and only VSIs will be analyzed in this system. Moreover, the common load is real-time varying and its components are unascertainable and uncontrollable, so the common load is described as $Z_{\text{load}}(s)$ in *s*-domain in the following equations.

As shown in this figure, letter a represents any VSI in the system. $V_{o.a}$ and $I_{o.a}$ are the output voltage and current of any VSI, respectively, and $Z_{w.a}$ is the wire impedance connecting this VSI and ac bus. U_{bus} is the voltage of ac bus, which also equals the voltage of Z_{load}, and I_{load} is the current of Z_{load}.

The *s*-domain modeling of VSIPS can be obtained based on this equivalent circuit. The expressions of $I_{o.a}$ and I_{load} can be expressed by (1) and (2), and the relationship of $I_{o.a}$ and I_{load} is given in (3)

$$I_{o.a}(s) = \frac{V_{o.a}(s) - U_{\text{bus}}(s)}{Z_{w.a}} \ (a = 1, ..., n) \tag{1}$$

$$I_{\text{load}}(s) = \frac{U_{\text{bus}}(s)}{Z_{\text{load}}(s)} \tag{2}$$

$$I_{\text{load}}(s) = \sum_{j=1}^{n} I_{o.j}(s). \tag{3}$$

According to these equations, the expression of U_{bus} can be obtained as (4). Then, the expression of $I_{o.a}$ can be obtained as (5) by substituting (4) into (1). Equations (1)–(5) can be regarded

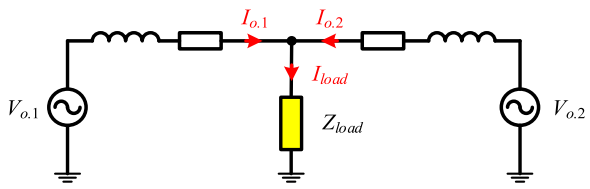

Fig. 2. VSIPS consisting of two VSIs.

as the fundamental mathematical description of VSIPS

$$U_{\text{bus}}(s)=\frac{\frac{V_{o.1}(s)}{Z_{w.1}}+\frac{V_{o.2}(s)}{Z_{w.2}}+\cdots+\frac{V_{o.n}(s)}{Z_{w.n}}}{\frac{1}{Z_{\text{load}}(s)}+\frac{1}{Z_{w.1}}+\frac{1}{Z_{w.2}}+\cdots+\frac{1}{Z_{w.n}}} \tag{4}$$

$$I_{o.a}(s)=\frac{\frac{1}{Z_{w.a}}\left[\frac{V_{o.a}(s)}{Z_{\text{load}}(s)}+\sum_{j=1}^{n}\frac{V_{o.a}(s)-V_{o.j}(s)}{Z_{w.j}}\right]}{\frac{1}{Z_{\text{load}}(s)}+\sum_{j=1}^{n}\frac{1}{Z_{w.j}}}. \tag{5}$$

According to (4) and (5), both U_{bus} and $I_{o.a}$ are controlled by all VSIs' voltages. Meanwhile, U_{bus} and $I_{o.a}$ are also influenced by the variation of Z_{load}. Therefore, considering that each VSI's voltage is controlled independently, it proves that VSIPS is a multi-input and multioutput system, which needs to be analyzed as an organic whole. In this system, the voltages of VSIs are the system inputs, and the output currents or the circulating currents of all VSIs can be defined as the system outputs. The wire impedance $Z_{w.a}$ of every VSI is a fixed parameter, Z_{load} is an uncontrollable variable, and U_{bus} is a state variable of VSIPS controlled by the voltages of all VSIs.

B. Definition of the Circulating Current

As shown in Fig. 2, the traditional definition of circulating currents can be expressed as (6), in which VSIPS consists of two VSIs and the load is shared equally [12]

$$\begin{cases} I_{\text{cir.1}}(s)=\dfrac{1}{2}\left[I_{o.1}(s)-I_{o.2}(s)\right] \\ I_{\text{cir.2}}(s)=\dfrac{1}{2}\left[I_{o.2}(s)-I_{o.1}(s)\right]. \end{cases} \tag{6}$$

Moreover, Zhang *et al.* [30] proposed the definition of the circulating current when VSIPS consisted of *n* VSI modules, as given in (7), but the definition is still not clear in the case when VSIs share the load with different ratios

$$I_{\text{cir.}a}(s)=I_{o.a}(s)-\frac{1}{n}I_{\text{load}}(s)\ (a=1,...,n). \tag{7}$$

In this paper, an accurate definition of the circulating current I_{cir} of VSIPS is proposed, which is given in (8). According to this equation, $I_{\text{cir.}a}$ is defined as the difference between the actual output current $I_{o.a}$ and the theoretical output current $I_{t.a}$. The theoretical output current $I_{t.a}$ is defined as the theoretical share of the load current for any VSI, as given in (9). In this equation, k_a is the weight coefficient of any VSI in load-power sharing, and it satisfies the relationship of (10). Therefore, the expression of I_{cir} can be obtained as (11)

$$I_{\text{cir.}a}(s)=I_{o.a}(s)-I_{t.a}(s)\ (a=1,...,n) \tag{8}$$

$$I_{t.a}(s)=k_a\cdot I_{\text{load}}(s)\ (a=1,...,n) \tag{9}$$

$$\sum_{j=1}^{n}k_j=1 \tag{10}$$

$$I_{\text{cir.}a}(s)=I_{o.a}(s)-k_a\cdot I_{\text{load}}(s)\ (a=1,...,n). \tag{11}$$

According to the proposed definition, $I_{\text{cir.}a}$ varies with k_a, which means I_{cir} is a virtual physical quantity. It is different from the traditional definition, in which I_{cir} is recognized as a real physical quantity. Usually, k_a is directly equivalent to the ratio of the rated output power of any VSI and the VSIPS by default, which can optimize output power sharing of VSIPS based on the output power capacity of each VSI.

C. Mathematical Descriptions of the Circulating Current and the Steady State

According to the definition, $I_{\text{cir.}a}$ can be expressed as (12), after the simplification by substituting (2), (4), and (5) into (11). This equation proves that $I_{\text{cir.}a}$ is directly controlled by all VSIs' voltages and also influenced by Z_{load} and Z_w. Meanwhile, $I_{\text{cir.}a}$ is real-time varying since Z_{load} is varying with time

$$I_{\text{cir.}a}(s)=\frac{V_{o.a}(s)}{Z_{w.a}}-\left(\frac{\frac{1}{Z_{w.a}}+\frac{k_a}{Z_{\text{load}}(s)}}{\sum_{j=1}^{n}\frac{1}{Z_{w.j}}+\frac{1}{Z_{\text{load}}(s)}}\right)\cdot\sum_{j=1}^{n}\frac{V_{o.j}(s)}{Z_{w.j}}. \tag{12}$$

In this paper, the steady state of VSIPS is defined as the case when the circulating currents of all VSI modules is equal to zero. This is a theoretical and ideal state, and it does not exist in the real world, but it is the final purpose of the parallel-operation control of VSIPS. Therefore, the relationship of VSIs' voltages in the steady state can be obtained as given in (13), which proves that this relationship will be affected by the change of Z_{load}

$$V_{o.a}(s)=Z_{w.a}\cdot\left(\frac{\frac{1}{Z_{w.a}}+\frac{k_a}{Z_{\text{load}}(s)}}{\sum_{j=1}^{n}\frac{1}{Z_{w.j}}+\frac{1}{Z_{\text{load}}(s)}}\right)\cdot\sum_{j=1}^{n}\frac{V_{o.j}(s)}{Z_{w.j}}\ (I_{\text{cir.}a}=0). \tag{13}$$

Equations (12) and (13) are the mathematical descriptions of the circulating current and the steady state of VSIPS. They prove that the load variation will lead to the change of circulating currents, and the steady state of VSIPS will be disrupted. Subsequently, all VSIs will adjust their voltages under the parallel-operation control in order to eliminate the circulating currents until a new steady state is established. However, the new steady state is very fragile, because Z_{load} is real-time changing. Therefore, the influence of the load variation must be eliminated. In order to solve this problem, an optimized mathematical model of VSIPS is proposed, which will be presented in the next section.

III. Proposed Optimized Mathematical Model of VSIPS

A. Optimum Design of the Wire Impedance

According to (12) and (13), Z_{load} only exists in a common factor of these two equations, which are defined as A as given in (14). And A can be rewritten in (15) by substituting (10) into (14)

$$A = \frac{\frac{1}{Z_{w.a}} + \frac{k_a}{Z_{\text{load}}(s)}}{\sum_{j=1}^{n} \frac{1}{Z_{w.j}} + \frac{1}{Z_{\text{load}}(s)}} \tag{14}$$

$$A = k_a \cdot \frac{\frac{1}{k_a Z_{w.a}} + \frac{1}{Z_{\text{load}}(s)}}{\sum_{j=1}^{n} \left[k_j \left(\frac{1}{k_j Z_{w.j}} + \frac{1}{Z_{\text{load}}(s)}\right)\right]}. \tag{15}$$

Therefore, if the wire impedance $Z_{w.a}$ of any VSI can satisfy (16), then (15) can be simplified into (17), which means the influence of Z_{load} is eliminated from (12) and (13). Thus, the relation of (16) can be defined as the optimum design of the wire impedance, in which the product of the wire impedance and weighted coefficient of any VSI is equal to Z_e. Meanwhile, Z_e is defined as the equivalent wire impedance of VSIPS, and its equivalent weighted coefficient is defined as 1

$$k_a \cdot Z_{w.a} = 1 \cdot Z_e \ (a = 1, ..., n) \tag{16}$$

$$A = k_a. \tag{17}$$

B. Optimized Fundamental Mathematical Description of VSIPS

Based on the optimum design of the wire impedance, the fundamental mathematical description of VSIPS can be further simplified. The expressions of U_{bus}, $I_{o.a}$, and I_{load} can be simplified as (18)–(20), respectively. In these equations, V_m is the weighted average of all VSIs' voltages in VSIPS, as given in (21)

$$U_{\text{bus}}(s) = \frac{Z_{\text{load}}(s)}{Z_e + Z_{\text{load}}(s)} \cdot V_m(s) \tag{18}$$

$$I_{o.a}(s) = \frac{1}{Z_{w.a}} \left[V_{o.a}(s) - \frac{Z_{\text{load}}(s)}{Z_e + Z_{\text{load}}(s)} V_m(s)\right] \tag{19}$$

$$I_{\text{load}}(s) = \frac{1}{Z_e + Z_{\text{load}}(s)} \cdot V_m(s) \tag{20}$$

$$V_m(s) = \sum_{j=1}^{n} [k_j \cdot V_{o.j}(s)]. \tag{21}$$

C. Optimized Mathematical Model of Circulating Current

Based on the optimum design of wire impedance, the expression of the circulating current can be simplified as (22) or (23) by substituting (19) and (20) into (11), which is the mathematical model of circulating current proposed in this paper. This model proves that if $Z_{w.a}$ satisfies the relation of (16), then $I_{\text{cir}.a}$ is only generated by the difference between $V_{o.a}$ and V_m; therefore, the value of $I_{\text{cir}.a}$ is determined by voltage difference and wire impedance, and the impact of Z_{load} on $I_{\text{cir}.a}$ is eliminated

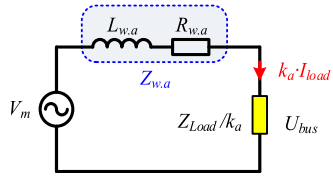

Fig. 3. Steady-state model of any VSI.

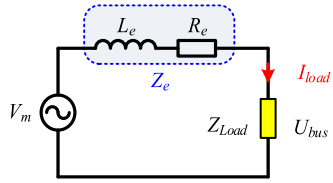

Fig. 4. Steady-state model of VSIPS.

$$I_{\text{cir}.a}(s) = \frac{V_{o.a}(s) - V_m(s)}{Z_{w.a}} \tag{22}$$

$$I_{\text{cir}.a}(s) = k_a \cdot \frac{V_{o.a}(s) - V_m(s)}{Z_e}. \tag{23}$$

D. Optimized Steady-State Model of VSIPS

According to the steady-state definition of VSIPS, (22) or (23) proves that every VSI's voltage equals V_m in the steady state, as given in (24). Therefore, V_m can be defined as the steady-state voltage of VSIPS. Meanwhile, the variation of Z_{load} has no influence on the steady state of VSIPS in this optimized model

$$V_{o.a}(s) = V_m(s) \ (\text{When } I_{\text{cir}.a} = 0). \tag{24}$$

The expression of $I_{o.a}$ can be further simplified as (25) by substituting (24) into (19) in the steady state. Meanwhile, by comparing (20) and (25), the relationship of I_{load} and $I_{o.a}$ in the steady state can be obtained as (26)

$$I_{o.a}(s) = \frac{1}{Z_{w.a} + \frac{Z_{\text{load}}(s)}{k_a}} \cdot V_m(s) \tag{25}$$

$$I_{o.a}(s) = k_a \cdot I_{\text{load}}(s). \tag{26}$$

Subsequently, based on the overall analysis of (24)–(26), the steady-state model of any VSI module can be obtained as shown in Fig. 3. In this model, the voltage of every VSI equals V_m, $Z_{w.a}$ is the wire impedance of every VSI, and Z_{load}/k_a is the shared load of every VSI. Meanwhile, the voltage of the shared load equals U_{bus}.

According to the steady-state model of any VSI module, the steady-state model of VSIPS can be obtained, as shown in Fig. 4. In this model, the whole system is equivalent to a single VSI module. Z_e is the equivalent wire impedance of this VSI, and the load of this VSI is the common load Z_{load}. Meanwhile, the voltage of Z_{load} equals U_{bus}.

Comparing Fig. 3 with Fig. 4 and considering the optimum design of the wire impedance, the steady-state models of any VSI and VSIPS are identical in essence. Therefore, the analysis

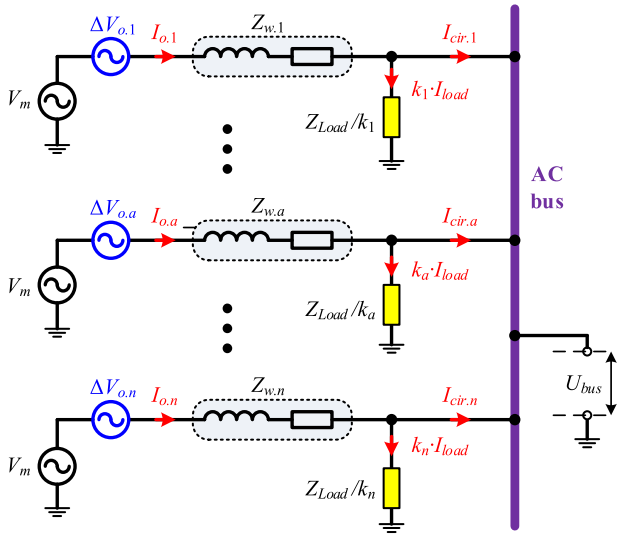

Fig. 5. Steady-state model with small-signal disturbance of VSIPS.

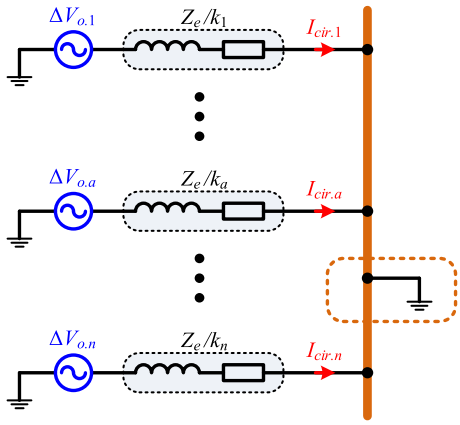

Fig. 6. Circulating-current small-signal model of VSIPS.

of any VSI in the steady state can be equivalent to the analysis of VSIPS.

E. Optimized Circulating-Current Small-Signal Model of VSIPS

Small-signal model of VSIPS can be obtained based on the further analysis of the steady-state model. Assuming that there is a small-signal disturbance $\Delta V_{o.a}$ in any VSI's voltage $V_{o.a}$ in the steady state, $V_{o.a}$ can be expressed as (27). According to the relationship between $V_{o.a}$ and V_m, as given in (21), (28) can be obtained

$$V_{o.a}(s) = V_m(s) + \Delta V_{o.a}(s) \tag{27}$$

$$\sum_{j=1}^{n} [k_j \cdot \Delta V_{o.j}(s)] = 0. \tag{28}$$

Moreover, the expressions of $I_{o.a}$ and $I_{\text{cir}.a}$ can be obtained as given in (29) and (30), by substituting (27) into (19) and (22). These two equations prove that $I_{\text{cir}.a}$ is generated by the small-signal disturbance of $V_{o.a}$, and $I_{\text{cir}.a}$ also can be recognized as the small-signal disturbance of $I_{o.a}$

$$I_{o.a}(s) = k_a \cdot I_{\text{load}}(s) + \frac{\Delta V_{o.a}(s)}{Z_{w.a}} \tag{29}$$

$$I_{\text{cir}.a}(s) = \frac{\Delta V_{o.a}(s)}{Z_{w.a}}. \tag{30}$$

Therefore, according to (29) and (30), the steady-state model with small-signal disturbance of VSIPS can be illustrated in Fig. 5. Subsequently, the circulating-current small-signal model of VSIPS can be obtained based on Fig. 6, in which all the steady-state signals are eliminated from Fig. 5.

F. Summary

In this section, the mathematical model of circulating current, steady-state model of VSIPS, and circulating-current small-signal model of VSIPS are proposed based on the optimum design of the wire impedance. These three models constitute the proposed optimized mathematical model of VSIPS in s-domain, which is the theoretical basis of this paper.

IV. Proposed Phasor Model of Circulating Current and CCP

A. Phasor Description of VSIPS

A fixed reference frequency is the basis of the phasor system. In this section, the reference frequency is set as the fundamental frequency of VSIs' voltage. Moreover, if it is set as a harmonic frequency, then the analysis of the section can be used to analyze the relative harmonic component of the circulating current.

According to the optimized steady-state model and small-signal model of VSIPS, $V_{o.a}$ of any VSI equals approximately to the steady-state voltage V_m in the steady state, and the difference $\Delta V_{o.a}$ of $V_{o.a}$, and V_m is regarded as the small-signal disturbance. So, the reference frequency is set as the angle frequency ω of V_m, and the following analysis can only apply for the steady state of VSIPS.

Based on the above-mentioned assumption, $\vec{V}_m$ and $\vec{V}_{o.a}$ can be expressed as (31) in the phasor model. V_A is the effective value of $\vec{V}_m$, and the phase of $\vec{V}_m$ is defined as 0. $V_{\text{rms}.a}$ is the effective value of $\vec{V}_{o.a}$, and θ_a is phase difference between $\vec{V}_m$ and $\vec{V}_{o.a}$. Therefore, (21) can be expressed as (32) in the phasor model

$$\begin{cases} \vec{V}_m = V_A \angle 0 \\ \vec{V}_{o.a} = V_{\text{rms}.a} \angle \theta_a \end{cases} \tag{31}$$

$$\vec{V}_m = \sum_{i=1}^{n} \left(k_i \cdot \vec{V}_{o.i} \right). \tag{32}$$

Equation (33) can be obtained by substituting (31) into (32). Because θ_a and "$V_{\text{rms}.a} - V_A$" are equal to 0 approximately,

(34) can be obtained after simplification

$$V_A = \sum_{i=1}^{n} (k_i \cdot V_{\text{rms}.i} \cos\theta_i) + j \sum_{i=1}^{n} (k_i \cdot V_{\text{rms}.i} \sin\theta_i) \quad (33)$$

$$\begin{cases} \sum_{i=1}^{n} (k_i \cdot V_{\text{rms}.i}) = V_A \\ \sum_{i=1}^{n} (k_i \cdot \theta_i) = 0. \end{cases} \quad (34)$$

$\vec{Z}_{w.a}$ and $\vec{Z}_e$ can be expressed as (35) and (36). $Z_{\text{rms}.a}$ and $\phi_{w.a}$ are the amplitude and phase of $\vec{Z}_{w.a}$, respectively, and $R_{w.a}$ and $L_{w.a}$ are the resistance and inductance of $\vec{Z}_{w.a}$, respectively. Z_E and ϕ_e are the amplitude and phase of $\vec{Z}_e$, respectively, and R_e and L_e are the resistance and inductance of $\vec{Z}_e$, respectively. The relationship of $\vec{Z}_{w.a}$ and $\vec{Z}_e$ complies with the relation of (37), which is obtained based on (16)

$$\vec{Z}_{w.a} = Z_{\text{rms}.a} \angle \phi_{w.a} = R_{w.a} + j\omega L_{w.a} \quad (35)$$

$$\vec{Z}_e = Z_E \angle \phi_e = R_e + j\omega L_e \quad (36)$$

$$\begin{cases} \phi_e = \phi_{w.a} \\ Z_E = k_a \cdot Z_{\text{rms}.a} \\ R_e = k_a \cdot R_{w.a} \\ L_e = k_a \cdot L_{w.a}. \end{cases} (a = 1, ..., n). \quad (37)$$

Moreover, the expression of $\vec{U}_{\text{bus}}$ and $\vec{I}_{\text{load}}$ is givenin (38) and (39), which are obtained based on (18) and (20)

$$\vec{U}_{\text{bus}} = \frac{\vec{Z}_{\text{load}}}{\vec{Z}_e + \vec{Z}_{\text{load}}} \vec{V}_m \quad (38)$$

$$\vec{I}_{\text{load}} = \frac{\vec{V}_m}{\vec{Z}_e + \vec{Z}_{\text{load}}}. \quad (39)$$

B. Phasor Model of Circulating Current

The phasor expression of $\vec{I}_{\text{cir}.a}$ is given in (40) based on the steady-state model and small-signal model. The small-signal disturbance $\Delta\vec{V}_{o.a}$ also complies with the relationship of (41) based on (28)

$$\vec{I}_{\text{cir}.a} = \frac{\vec{V}_{o.a} - \vec{V}_m}{\vec{Z}_{w.a}} = k_a \frac{\Delta\vec{V}_{o.a}}{\vec{Z}_e} \quad (40)$$

$$\sum_{i=1}^{n} \left(k_i \cdot \Delta\vec{V}_{o.i}\right) = 0. \quad (41)$$

By substituting (31) into (27), (42) is obtained. The phase difference θ_a and the voltage difference $V_{\text{rms}.a} - V_A$ between $\vec{V}_{o.a}$ and $\vec{V}_m$ are both infinitesimal, so $\sin\theta_a$ equals θ_a and $\cos\theta_a$ equals 1 approximately. Meanwhile, the product of $\sin\theta_a$ and $V_{\text{rms}.a} - V_A$ is a second-order infinitesimal comparing with θ_a and $V_{\text{rms}.a} - V_A$, which can be eliminated from (42); thus, the phasor expression of $\Delta\vec{V}_{o.a}$ can be simplified from the following equations:

$$\Delta\vec{V}_{o.a} = V_{\text{rms}.a} \cos\theta_a - V_A + j\left[V_{\text{A}} \sin\theta_a + (V_{\text{rms}.a} - V_{\text{A}}) \sin\theta_a\right] \quad (42)$$

$$\Delta\vec{V}_{o.a} = V_{\text{rms}.a} - V_A + jV_A\theta_a. \quad (43)$$

Subsequently, the phasor expression of $\vec{I}_{\text{cir}.a}$ can be obtained as given in (44) and (45) by subsisting (36) and (43) into (40), and $I_{\text{cir}.a.p}$ and $I_{\text{cir}.a.q}$ are the real component and imaginary component of $\vec{I}_{\text{cir}.a}$, respectively

$$\vec{I}_{\text{cir}.a} = I_{\text{cir}.a.p} + j \cdot I_{\text{cir}.a.q} \quad (44)$$

$$\begin{cases} I_{\text{cir}.a.p} = k_a \cdot \dfrac{(V_{\text{rms}.a} - V_A)\cos\phi_e + \theta_a V_A \sin\phi_e}{Z_E} \\ I_{\text{cir}.a.q} = k_a \cdot \dfrac{\theta_a V_A \cos\phi_e - (V_{\text{rms}.a} - V_A)\sin\phi_e}{Z_E}. \end{cases} \quad (45)$$

Equations (44) and (45) are defined as the phasor model of the circulating current. It proves that $I_{\text{cir}.a.p}$ and $I_{\text{cir}.a.q}$ are controlled by voltage difference $V_{\text{rms}.a} - V_A$ and phase difference θ_a simultaneously. This coupling relationship is affected by phase ϕ_e of $\vec{Z}_e$.

Furthermore, the phasor model can be simplified as (46) or (47) when ϕ_e equals 0° or 90°, respectively. They express that $I_{\text{cir}.a.p}$ is directly controlled by $V_{\text{rms}.a} - V_A$, $I_{\text{cir}.a.q}$ is directly controlled by θ_a in the pure resistive wire impedance, $I_{\text{cir}.a.p}$ is directly controlled by θ_a, and $I_{\text{cir}.a.q}$ is directly controlled by $V_{\text{rms}.a} - V_A$ in the pure inductive wire impedance

$$\begin{cases} I_{\text{cir}.a.p} = \dfrac{k_a}{R_e} \cdot (V_{\text{rms}.a} - V_A) \\ I_{\text{cir}.a.q} = \dfrac{k_a V_A}{R_e} \cdot \theta_a \end{cases} \quad (\text{When } \phi_e = 0^\circ) \quad (46)$$

$$\begin{cases} I_{\text{cir}.a.p} = \dfrac{k_a V_A}{L_e} \cdot \theta_a \\ I_{\text{cir}.a.q} = -\dfrac{k_a}{L_e} \cdot (V_{\text{rms}.a} - V_A). \end{cases} \quad (\text{When } \phi_e = 90^\circ). \quad (47)$$

C. Phasor Model of CCP

According to the small-signal model of VSIPS, the complex output power $\vec{S}_{o.a}$ of any VSI in phasor model can be expressed as (48). Meanwhile, according to (40), (48) can be transformed into (49)

$$\vec{S}_{o.a} = \vec{V}_{o.a} \cdot \vec{I}^*_{o.a} = \left(\vec{V}_m + \Delta\vec{V}_{o.a}\right) \cdot \left(k_a \cdot \vec{I}_{\text{load}} + \vec{I}_{\text{cir}.a}\right)^* \quad (48)$$

$$\vec{S}_{o.a} = k_a \cdot \vec{V}_m \vec{I}^*_{\text{load}} + k_a \Delta\vec{V}_{o.a} \cdot \vec{I}^*_{\text{load}} + k_a \Delta\vec{V}^*_{o.a} \cdot \frac{\vec{V}_m}{\vec{Z}^*_e} + k_a \cdot \frac{\Delta\vec{V}_{o.a} \cdot \Delta\vec{V}^*_{o.a}}{\vec{Z}^*_e}. \quad (49)$$

In (49), $\Delta\vec{V}_{o.a} \cdot \Delta\vec{V}^*_{o.a}$ is a second-order infinitesimal comparing to $\Delta\vec{V}_{o.a}$. Therefore, (49) can be simplified as the following eqaution:

$$\vec{S}_{o.a} = k_a \cdot \vec{V}_m \vec{I}^*_{\text{load}} + k_a \Delta\vec{V}_{o.a} \cdot \vec{I}^*_{\text{load}} + k_a \Delta\vec{V}^*_{o.a} \cdot \frac{\vec{V}_m}{\vec{Z}^*_e}. \quad (50)$$

Moreover, the relation of VSI's complex power $\vec{S}_{o.a}$ and VSIPS's complex power $\vec{S}_{\text{to}}$ can be expressed as (51) in the

phasor model. Subsequently, (52) can be obtained by substituting (50) into (51)

$$\vec{S}_{\text{to}} = \sum_{i=1}^{n} \vec{S}_{o.i} \tag{51}$$

$$\vec{S}_{\text{to}} = \vec{V}_m \cdot \vec{I}^*_{\text{load}} \cdot \sum_{i=1}^{n} k_i + \vec{I}^*_{\text{load}} \cdot \sum_{i=1}^{n} \left(k_i \cdot \Delta \vec{V}_{o.i} \right) + \frac{\vec{V}_m}{\vec{Z}^*_e} \cdot \sum_{i=1}^{n} \left(k_i \cdot \Delta \vec{V}^*_{o.i} \right). \tag{52}$$

According to (10) and (41), (52) can be further simplified as (53). This simplified equation is an important conclusion for the phasor model of VSIPS, which proves that the complex power $\vec{S}_{\text{to}}$ of VSIPS equals the product of $\vec{V}_m$ and $\vec{I}_{\text{load}}$ in the steady state

$$\vec{S}_{\text{to}} = \vec{V}_m \cdot \vec{I}^*_{\text{load}}. \tag{53}$$

Meanwhile, $\vec{S}_{o.a}$ can be defined as (54) based on (50) and (53), which proves that $\vec{S}_{o.a}$ equals the sum of the theoretical output power and the CCP $\vec{S}_{\text{cir}.a}$. The theoretical output power equals the product of k_a and $\vec{S}_{\text{to}}$, and $\vec{S}_{\text{cir}.a}$ can be expressed as (55) based on (50) and (53)

$$\vec{S}_{o.a} = k_a \cdot \vec{S}_{\text{to}} + \vec{S}_{\text{cir}.a} \tag{54}$$

$$\vec{S}_{\text{cir}.a} = k_a \cdot \Delta \vec{V}_{o.a} \cdot \vec{I}^*_{\text{load}} + \vec{V}_m \cdot \left(k_a \frac{\Delta \vec{V}_{o.a}}{\vec{Z}_e} \right)^*. \tag{55}$$

Therefore, (56) can be obtained after simplification by substituting (31), (36), (39), and (43) into (55). The expressions of S_1, S_2, and S_3 are given in (57). Furthermore, S_3 is a second-order infinitesimal due to the product of θ_a and $V_{\text{rms}.a} - V_A$, so it is far smaller than S_1 and S_2, and can be eliminated from (56).

Equations (56) and (57) prove that $\vec{Z}_{\text{load}}$ will affect the expression of $\vec{S}_{\text{cir}.a}$. So, it is impossible to obtain the accurate expression of $\vec{S}_{\text{cir}.a}$, since the expression of $\vec{Z}_{\text{load}}$ is not only unclear but also real-time changing. Therefore, the influence of $\vec{Z}_{\text{load}}$ must be eliminated in order to obtain the mathematical model of the CCP

$$\vec{S}_{\text{cir}.a} = S_1 + j\left(S_2 + S_3\right) \tag{56}$$

$$\begin{cases} S_1 = k_a \cdot V_A \cdot (V_{\text{rms}.a} - V_A) \cdot \left(\dfrac{1}{\vec{Z}^*_e + \vec{Z}^*_{\text{load}}} + \dfrac{1}{\vec{Z}^*_e} \right) \\ S_2 = k_a \cdot V_A^2 \cdot \theta_a \left(\dfrac{1}{\vec{Z}^*_e + \vec{Z}^*_{\text{load}}} - \dfrac{1}{\vec{Z}^*_e} \right) \\ S_3 = (V_{\text{rms}.a} - V_A) \cdot \theta_a \cdot k_a \cdot V_A \cdot \left(\dfrac{1}{\vec{Z}^*_e + \vec{Z}^*_{\text{load}}} - \dfrac{1}{\vec{Z}^*_e} \right). \end{cases} \tag{57}$$

According to (56) and (57), if the value of $\vec{Z}_e$ is far smaller than $\vec{Z}_{\text{load}}$, then the relationship of (58) can be realized, and the expression of $\vec{S}_{\text{cir}.a}$ can be obtained after simplification as given in (59), in which the influence of $\vec{Z}_{\text{load}}$ is eliminated

$$\left| \frac{1}{\vec{Z}^*_e + \vec{Z}^*_{\text{load}}} \right| << \left| \frac{1}{\vec{Z}^*_e} \right| \tag{58}$$

$$\vec{S}_{\text{cir}.a} = (V_{\text{rms}.a} - V_A) \cdot k_a \cdot V_A \cdot \frac{1}{\vec{Z}^*_e} - j \cdot \theta_a \cdot k_a \cdot V_A^2 \cdot \frac{1}{\vec{Z}^*_e}. \tag{59}$$

Meanwhile, the variation range of $\vec{Z}_{\text{load}}$ can be obtained according to the rated power of VSIs, which can be expressed as (60). $\vec{Z}_d$ is the equivalent load at the rated power of VSIPS, and its expression is (61). S_{TA} is the total rated output power of VSIPS and equals the sum of the rated output power $S_{\text{RA}.a}$ of all VSIs

$$\left| \vec{Z}_d \right| \le \left| \vec{Z}_{\text{load}} \right| \le +\infty \tag{60}$$

$$\left| \vec{Z}_d \right| = \frac{V_A^2}{S_{\text{TA}}} = k_a \frac{V_A^2}{S_{\text{RA}.a}} \ (a = 1, ..., n). \tag{61}$$

Therefore, the optional range of $\vec{Z}_e$ can be obtained according to the variation range of $\vec{Z}_{\text{load}}$. In this paper, if the value of $\vec{Z}_e$ is smaller than 1/50 of the value of $\vec{Z}_{\text{load}}$, then it is observed that $\vec{Z}_e$ is far smaller than $\vec{Z}_{\text{load}}$, and the influence of $\vec{Z}_{\text{load}}$ is regarded to be eliminated. Thus, the optional range of $\vec{Z}_e$ can be expressed as the following eqaution:

$$\left| \vec{Z}_e \right| \le \frac{V_A^2}{50 \cdot S_{\text{TA}}}. \tag{62}$$

After the influence of $\vec{Z}_{\text{load}}$ is eliminated, $\vec{S}_{\text{cir}.a}$ can be expressed as (63) and (64) by substituting (36) into (59). In (63) and (64), $P_{\text{cir}.a}$ and $Q_{\text{cir}.a}$ are the active and reactive CCP of any VSI, respectively

$$\vec{S}_{\text{cir}.a} = P_{\text{cir}.a} + j \cdot Q_{\text{cir}.a} \tag{63}$$

$$\begin{cases} P_{\text{cir}.a} = \dfrac{k_a V_A}{\omega^2 L_e^2 + R_e^2} \left[R_e \left(V_{\text{rms}.a} - V_A \right) + \theta_a V_A \omega L_e \right] \\ Q_{\text{cir}.a} = \dfrac{k_a V_A}{\omega^2 L_e^2 + R_e^2} \left[\omega L_e \left(V_{\text{rms}.a} - V_A \right) - \theta_a V_A R_e \right]. \end{cases} \tag{64}$$

Equations (63) and (64) are defined as the CCPPM. According to this model, $P_{\text{cir}.a}$ and $Q_{\text{cir}.a}$ are controlled by voltage difference $V_{\text{rms}.a} - V_A$ and phase difference θ_a simultaneously. This coupling relationship is affected by the phase ϕ_e of $\vec{Z}_e$.

Meanwhile, the phasor model can be simplified as (65) or (66) when ϕ_e equals 0° or 90°. These two equations show that $P_{\text{cir}.a}$ is directly controlled by $V_{\text{rms}.a} - V_A$ and $Q_{\text{cir}.a}$ is directly controlled by θ_a in the pure resistive wire impedance, and $P_{\text{cir}.a}$ is directly controlled by θ_a and $Q_{\text{cir}.a}$ is directly controlled by

$V_{\text{rms}.a} - V_A$ in the pure inductive wire impedance

$$\begin{cases} P_{\text{cir}.a} = \dfrac{k_a V_A}{R_e}\left(V_{\text{rms}.a} - V_A\right) \\ Q_{\text{cir}.a} = \dfrac{k_a V_A^2}{R_e} \cdot (-\theta_a) \end{cases} \quad (\text{When } \phi_e = 0^\circ) \tag{65}$$

$$\begin{cases} P_{\text{cir}.a} = \dfrac{k_a V_A^2}{\omega L_e} \cdot \theta_a \\ Q_{\text{cir}.a} = \dfrac{k_a V_A}{\omega L_e} \cdot \left(V_{\text{rms}.a} - V_A\right) \end{cases} \quad (\text{When } \phi_e = 90^\circ). \tag{66}$$

Moreover, $P_{\text{cir}.a}$ and $Q_{\text{cir}.a}$ also comply with the relationship of (67), which can be obtained based on (51) and (54). In this equation, $P_{o.a}$ and $Q_{o.a}$ are the active and reactive output power of any VSI, respectively, and P_{to} and Q_{to} are the total active and reactive power of VSIPS

$$\begin{cases} P_{o.a} = k_a \cdot P_{\text{to}} + P_{\text{cir}.a} = k_a \cdot \sum_{i=1}^{n} P_{o.i} + P_{\text{cir}.a} \\ Q_{o.a} = k_a \cdot Q_{\text{to}} + Q_{\text{cir}.a} = k_a \cdot \sum_{i=1}^{n} Q_{o.i} + Q_{\text{cir}.a} \end{cases}. \tag{67}$$

V. Modeling and Analysis of Traditional Droop Control

A. Control Equations of Traditional Droop Control

Traditional droop control can be named as $\omega - P$ and $V - Q$ control when the wire impedance is inductive[1]– [3], and (68) presents the principle of $\omega - P$ and $V - Q$ control in every control cycle. ω^* and V^* are the rated angular frequency and effective value of all VSIs' voltages, $m_{\omega.a}$ and $n_{v.a}$ are the droop coefficients of any VSI that satisfies the relation of (69), and $m_{\omega.e}$ and $n_{v.e}$ are defined as the equivalent droop coefficient

$$\begin{cases} \omega_{a.k} = \omega^* - m_{\omega.a} \cdot P_{o.a.k-1} \\ V_{a.k} = V^* - n_{v.a} \cdot Q_{o.a.k-1} \end{cases} \tag{68}$$

$$\begin{cases} m_{\omega.a} \cdot k_a = m_{\omega.e} \\ n_{v.a} \cdot k_a = n_{v.e} \end{cases} (a = 1, ..., n). \tag{69}$$

In (68), *k* represents the serial number of control cycle in (68). $P_{o.a.k-1}$ and $Q_{o.a.k-1}$ are the active and reactive output power of any VSI in the $(k-1)$th cycle, $\omega_{a.k}$ and $V_{a.k}$ are the angular frequency and effective value of any VSI's voltage $\vec{V}_{o.a}$, which are adjusted by droop control in the kth cycle.

Since the frequency variation of any VSI module is regarded as a small-signal disturbance in the steady state, $\omega - P$ control can be transformed to $\theta - P$ control based on the fixed reference frequency ω^* in the phasor system, as given in (70). In this equation, $T_{c.\omega}$ is the time of $\omega - P$ control cycle, and $\theta_{a.k}$ is the adjusted phase by droop control in the kth cycle

$$\theta_{a.k} = \theta_{a.k-1} - m_{\omega.a} \cdot T_{c.\omega} \cdot P_{o.a.k-1}. \tag{70}$$

Moreover, it is assumed that the droop control is activated from the first cycle in the analysis, and the zeroth control cycle is the initial state. The initial angle frequency equals ω^*, and the initial phase $\theta_{a.0}$ and the effective value $V_{a.0}$ of every VSI is assumed as θ_a and $V_{\text{rms}.a}$. Meanwhile, the steady-state voltage in the initial state is assumed as $\vec{V}_m$.

As mentioned in Section I, the voltages of VSIs are different from each other even though all VSIs have the same voltage reference. Therefore, the control equation of $V - Q$ control should be adjusted by replacing the voltage reference V^* with $V_{\text{rms}.a}$, and it means that any VSI's voltage will be equal to $V_{\text{rms}.a}$ when the reference is set as V^*. Thus, the adjusted control equations of traditional droop control in the phasor model can be described as $\omega - P$, $\theta - P$, and $V - Q$ control, as given in the following eqaution:

$$\begin{cases} \omega_{a.k} = \omega^* - m_{\omega.a} \cdot P_{o.a.k-1}(\omega_{a.0} = \omega^*) \\ \theta_{a.k} = \theta_{a.k-1} - m_{\omega.a} \cdot T_{c.\omega} \cdot P_{o.a.k-1}(\theta_{a.0} = \theta_a) \\ V_{a.k} = V_{\text{rms}.a} - n_{v.a} \cdot Q_{o.a.k-1}(V_{a.0} = V_{\text{rms}.a}). \end{cases} \tag{71}$$

B. Steady-State Voltage of Traditional Droop Control

According to the relationship of (67), (71) can be transformed to (72) by substituting (67) and (69) into (71). In (72), $P_{\text{cir}.a.k-1}$ and $Q_{\text{cir}.a.k-1}$ are the circulating-current power in the $(k-1)$th cycle, P_{to} and Q_{to} are recognized as constants in the steady state

$$\begin{cases} \omega_{a.k} = \omega^* - m_{\omega.e} \cdot P_{to} - m_{\omega.a} \cdot P_{\text{cir}.a.k-1} \\ \theta_{a.k} = \theta_{a.k-1} - m_{\omega.e} \cdot T_{c.\omega} \cdot P_{to} - m_{\omega.a} T_{c.\omega} \cdot P_{\text{cir}.a.k-1} \\ V_{a.k} = V_{\text{rms}.a} - n_{v.e} \cdot Q_{to} - n_{v.a} \cdot Q_{\text{cir}.a.k-1}. \end{cases} \tag{72}$$

Equation (72) proves that the voltage of every VSI includes the same voltage bias caused by P_{to} and Q_{to}. Therefore, when the droop control is activated, the steady-state voltage of VSIPS will change from $\vec{V}_m$ to a new voltage defined as $\vec{V}_{m.d.k}$ due to the voltage bias. Comparing to $\vec{V}_m$, the angular frequency $\omega_{d.k}$, phase $\theta_{d.k}$ and effective value $V_{A.d.k}$ of $\vec{V}_{m.d.k}$ can be expressed as the following eqaution:

$$\begin{cases} \omega_{d.k} = \omega^* - m_{\omega.e} \cdot P_{\text{to}} \\ \theta_{d.k} = \theta_{d.k-1} - m_{\omega.e} \cdot T_{c.\omega} \cdot P_{\text{to}} \\ V_{A.d.k} = V_A - n_{v.e} \cdot Q_{\text{to}}. \end{cases} \tag{73}$$

Equation (73) expresses that the steady-state voltage bias is determined by droop coefficients and output power. Moreover, $\omega_{d.k}$ and $V_{A.d.k}$ are stable in the steady state, which are defined as ω_d and $V_{A.d}$ as given in (74), and $\theta_{d.k}$ varies with time ($t = k \cdot T_{c.\omega}$) because of the frequency bias. Meanwhile, $\vec{V}_{m.d.0}$ equals $\vec{V}_m$ at the zeroth control cycle, so $\theta_{d.0}$, $\omega_{d.0}$, and $V_{A.d.0}$ equal to 0, ω^*, and V_A, respectively. Therefore, the expression of $\vec{V}_{m.d.k}$ can be obtained as given in (75)

$$\begin{cases} \omega_d = \omega^* - m_{\omega.e} \cdot P_{to} \\ V_{A.d} = V_A - n_{v.e} \cdot Q_{to} \end{cases} \tag{74}$$

$$\begin{cases} \omega_{d.k} = \omega_d & (\omega_{d.0} = \omega^*) \\ \theta_{d.k} = \theta_{d.k-1} - m_{\omega.e} \cdot T_{c.\omega} \cdot P_{to} & (\theta_{d.0} = 0) \\ V_{A.d.k} = V_{A.d} & (V_{A.d.0} = V_A). \end{cases} \tag{75}$$

C. Mathematical Model of the Traditional Droop Control

According to the definition of (75), (72) can be transformed to (76). This new equation proves that, in every control cycle

of the droop method, every VSI module tries to adjust its phase difference and amplitude difference between $\vec{V}_{o.a}$ and $\vec{V}_{m.d.k}$ according to its own CCP $P_{\text{cir}.a.k-1}$ and $Q_{\text{cir}.a.k-1}$ in the previous control cycle. Therefore, this equation can be defined as the mechanism of the circulating-current elimination of droop control

$$\begin{cases} \theta_{a.k} - \theta_{d.k} = (\theta_{a.k-1} - \theta_{d.k-1}) - m_{\omega.e} T_{c.\omega} \cdot \dfrac{P_{\text{cir}.a.k-1}}{k_a} \\ V_{a.k} - V_{A.d} = (V_{\text{rms}.a} - V_A) - n_{v.e} \cdot \dfrac{Q_{\text{cir}.a.k-1}}{k_a}. \end{cases} \tag{76}$$

Equation (76) can be further analyzed by substituting the expression of $P_{\text{cir}.a}$ and $Q_{\text{cir}.a}$. Considering the steady-state voltage bias (ω_d) and the inductance wire impedance ($R_e = 0$) in the droop control, the expression of $P_{\text{cir}.a.k}$ and $Q_{\text{cir}.a.k}$ can be expressed as (77) according to CCPPM

$$\begin{cases} P_{\text{cir}.a.k} = \dfrac{k_a V_{A.d}^2}{\omega_d L_e} \cdot (\theta_{a.k} - \theta_{d.k}) \\ Q_{\text{cir}.a.k} = \dfrac{k_a V_{A.d}}{\omega_d L_e} \cdot (V_{a.k} - V_{A.d}). \end{cases} \tag{77}$$

After substituting (77) into (76), (78) can be obtained after simplification. This equation proves that $\theta_{\text{a.k}}$ and $V_{\text{a.k}}$ can be regarded as two first-order recurrence series, and (78) is the recurrence formulas of $\theta_{\text{a.k}}$ and $V_{\text{a.k}}$

$$\begin{cases} \theta_{a.k} - \theta_{d.k} = \left(1 - \dfrac{m_{\omega.e} T_{c.\omega} V_{A.d}^2}{\omega_d L_e}\right) \cdot (\theta_{a.k-1} - \theta_{d.k-1}) \\ V_{a.k} - V_{A.d} = (V_{\text{rms}.a} - V_A) - \dfrac{n_{v.e} V_{A.d}}{\omega_d L_e} \cdot (V_{a.k-1} - V_{A.d}) \end{cases} \tag{78}$$

$$\begin{cases} \theta_{a.k} = \theta_{d.k} + \left(1 - \dfrac{m_{\omega.e} T_{c.\omega} V_{A.d}^2}{\omega_d L_e}\right)^k \cdot \theta_a \\ V_{a.k} = V_{A.d} + \frac{\omega_d L_e (V_{\text{rms}.a} - V_A)}{n_{v.e} V_{A.d} + \omega_d L_e} \\ \qquad + \left(-\dfrac{n_{v.e} V_{A.d}}{\omega_d L_e}\right)^k \cdot \dfrac{n_{v.e} V_{A.d}}{n_{v.e} V_{A.d} + \omega_d L_e} (V_{\text{rms}.a} - V_A). \end{cases} \tag{79}$$

Subsequently, the mathematical solution of the recurrence series can be easily obtained, which is given in (79). Therefore, (79) is the general-term formula of $\theta_{a.k}$ and $V_{a.k}$, which describe the changing trend of the phase and effective value of every VSI's voltage. Therefore, this equation can be defined as the mathematical model of traditional droop control.

D. Analysis of Droop's Mathematical model

According to (79), $\theta_{a.k}$ and $V_{a.k}$ should be convergent sequences in order to ensure the stability of VSIPS. Therefore, the relationship of (80) should be complied with to make sure $\theta_{a.k}$ and $V_{a.k}$ are convergent. Concurrently, (81) can be obtained based on (80), which clarifies the optional range of the droop coefficients ($m_{\omega.e}$ and $n_{v.e}$) in traditional droop control

$$\begin{cases} -1 < \left(1 - \dfrac{m_{\omega.e} T_{c.\omega} V_{A.d}^2}{\omega_d L_e}\right) < 1 \\ -1 < \left(-\dfrac{n_{v.e} V_{A.d}}{\omega_d L_e}\right) < 1 \end{cases} \tag{80}$$

$$\begin{cases} 0 < m_{\omega.e} < \dfrac{2\omega_d L_e}{T_{c.\omega} V_{A.d}^2} \\ -\dfrac{\omega_d L_e}{V_{A.d}} < n_{v.e} < \dfrac{\omega_d L_e}{V_{A.d}}. \end{cases} \tag{81}$$

Moreover, according to (79), the convergent limits of $\theta_{a.k}$ and $V_{a.k}$ can obtained as given in (82). This equation proves that the phase of any VSI's voltage $\vec{V}_{o.a}$ will be equal to the phase of the new steady-state voltage $\vec{V}_{m.d.k}$ after a certain length of time, but there will be a fixed effective-value deviation between $\vec{V}_{o.a}$ and $\vec{V}_{m.d.k}$, and this deviation cannot be eliminated

$$\begin{cases} \lim\limits_{k\to\infty} \theta_{a.k} = \theta_{d.k} \\ \lim\limits_{k\to\infty} V_{a.k} = V_{A.d} + \dfrac{\omega_d L_e (V_{\text{rms}.a} - V_A)}{n_{v.e} V_{A.d} + \omega_d L_e}. \end{cases} \tag{82}$$

Meanwhile, the convergence limit of $P_{\text{cir}.a}$ and $Q_{\text{cir}.a}$ can be obtained by substituting (82) into (77), which is given in (83). This equation proves that, in the traditional droop control, $\omega - P$ control can eliminate the active CCP, but $V - Q$ control cannot eliminate the reactive CCP

$$\begin{cases} \lim\limits_{k\to\infty} P_{\text{cir}.a.k} = \lim\limits_{k\to\infty} \dfrac{k_a V_{A.d}^2 (\theta_{a.k} - \theta_{d.k})}{\omega_d L_e} = 0 \\ \lim\limits_{k\to\infty} Q_{\text{cir}.a.k} = \lim\limits_{k\to\infty} \dfrac{k_a V_{A.d} (V_{a.k} - V_{A.d})}{\omega_d L_e} \\ \qquad\qquad = \dfrac{k_a V_{A.d} (V_{\text{rms}.a} - V_A)}{n_{v.e} V_{A.d} + \omega_d L_e}. \end{cases} \tag{83}$$

Although $Q_{\text{cir}.a}$ cannot be eliminated, (83) proves that $Q_{\text{cir}.a}$ can be reduced by three methods: decreasing $V_{\text{rms}.a} - V_A$, increasing L_e, and increasing $n_{v.e}$. And the analysis of these methods is presented as follows.

1) Decreasing $V_{\text{rms}.a} - V_A$ means improving the control accuracy of VSI's voltage, so better output voltage control strategy and better hardware circuit are necessary for the design of VSI module, and the increase of cost is unavoidable.
2) Increasing L_e is easy to implement in the experiment, but it will increase the influence of Z_{load} on the droop control according to the analysis of CCPPM; simultaneously, the large inductor will deteriorate the quality of ac BUS voltage U_{bus}, and the volume and weight of large inductor are also troubles for the system design.
3) Increasing $n_{v.e}$ is the easiest way in the three methods. However, the range of $n_{v.e}$ is limited to ensure the stability of VSIPS as given in (81). Moreover, according to (74), the increase of $n_{v.e}$ will increase the amplitude bias of VSI's voltage. Therefore, the tradeoff of droop control between the steady-state voltage error and the load-sharing accuracy is elaborated by (74) and (83).

E. Summary

This section builds and analyzes the mathematical model of traditional droop control based on CCPPM, and proves that the droop control has the following two inborn deficiencies:

1) frequency and amplitude bias in the steady-state voltage, which are generated by output power and droop coefficients;
2) $V-Q$ droop control cannot realize accurate reactive-power sharing.

Moreover, the well-known tradeoff of the droop control, which is between the steady-state voltage bias and the load-sharing accuracy, is elaborated by the mathematical analysis of this section.

VI. Proposed Accurate Power-Sharing Control Method

A. Design of the Improved Control Method

In order to solve the deficiencies of traditional droop control, an improved control method is proposed in this section, which embodies two improvements. The first one is replacing the output power $P_{o.a}$ and $Q_{o.a}$ with the CCP $P_{\text{cir}.a}$ and $Q_{\text{cir}.a}$, respectively, in the droop control, which is used to eliminate the steady-state voltage bias. Another one is replacing the voltage reference V^* with the previous-cycle voltage $V_{a.k-1}$ in $V-Q$ control, which is used to realize the accurate reactive-power sharing.

Therefore, the control equations of the proposed method can be expressed as (84), which is named as $\omega-P_{\text{cir}}$ and $V-Q_{\text{cir}}$ control. In the phasor model, $\omega-P_{\text{cir}}$ control can be transformed to $\theta-P_{\text{cir}}$ control, as given in (85). Moreover, the definition of the initial state is the same as the droop control

$$\begin{cases}\omega_{a.k}=\omega^*-m_{\omega.a}\cdot P_{\text{cir}.a.k-1}(\omega_{a.0}=\omega^*)\\ V_{a.k}=V_{a.k-1}-n_{v.a}\cdot Q_{\text{cir}.a.k-1}(V_{a.0}=V_{\text{rms}.a})\end{cases}\tag{84}$$

$$\theta_{a.k}=\theta_{a.k-1}-m_{\omega.a}\cdot T_{c.\omega}\cdot P_{\text{cir}.a.k-1}\ (\theta_{a.0}=\theta_a).\tag{85}$$

B. Mathematical Model of the Proposed Control Method

The expression of $P_{\text{cir}.a}$ and $Q_{\text{cir}.a}$ can be simplified to (86) according to the inductance wire impedance ($R_e=0$). Moreover, since $P_{\text{cir}.a}$ and $Q_{\text{cir}.a}$ are the small-signal disturbances of $P_{o.a}$ and $Q_{o.a}$ in the steady state, it means no frequency bias or voltage bias will be generated in the proposed method, and the steady-state voltage will not change in the proposed method

$$\begin{cases}P_{\text{cir}.a.k}=\dfrac{k_aV_A^2}{\omega L_e}\cdot\theta_{a.k}\\ Q_{\text{cir}.a.k}=\dfrac{k_aV_A}{\omega L_e}\cdot(V_{a.k}-V_A).\end{cases}\tag{86}$$

After substituting (86) into the equations of $\theta-P_{\text{cir}}$ and $V-Q_{\text{cir}}$ control, (87) can be obtained. It proves that $\theta_{a.k}$ and $V_{a.k}$ are two first-order recurrence series, and (87) is the recurrence formulas of $\theta_{a.k}$ and $V_{a.k}$

$$\begin{cases}\theta_{a.k}=\theta_{a.k-1}-m_{\omega.e}T_{c.\omega}\cdot\dfrac{V_A^2}{\omega L_e}\cdot\theta_{a.k-1}\\ V_{a.k}=V_{a.k-1}-n_{v.e}\cdot\dfrac{V_A}{\omega L_e}\cdot(V_{a.k-1}-V_A).\end{cases}\tag{87}$$

Subsequently, the general term formulas of $\theta_{a.k}$ and $V_{a.k}$ can be obtained as given in (88). It elaborates the changing trend of the phase and effective value of every VSI's voltage. Therefore, it can be defined as the mathematical model of the proposed method

$$\begin{cases}\theta_{a.k}=\left(1-\dfrac{m_{\omega.e}T_{c.\omega}V_A^2}{\omega L_e}\right)^k\cdot\theta_a\\ V_{a.k}=V_A+\left(1-\dfrac{n_{v.e}V_A}{\omega L_e}\right)^k\cdot(V_{\text{rms}.a}-V_A).\end{cases}\tag{88}$$

C. Analysis of the Mathematical Model

According to (88), $\theta_{a.k}$ and $V_{a.k}$ should be convergent sequences in order to ensure the stability of VSIPS. Therefore, the relationship of (89) should be complied with to make sure that $\theta_{a.k}$ and $V_{a.k}$ are convergent. Concurrently, (90) can be obtained based on (89), which clarifies the optional range of the droop coefficients ($m_{\omega.e}$ and $n_{v.e}$) in proposed control method

$$\begin{cases}-1<\left(1-\dfrac{m_{\omega.e}T_{c.\omega}V_A^2}{\omega L_e}\right)<1\\ -1<\left(1-\dfrac{n_{v.e}V_A}{\omega L_e}\right)<1\end{cases}\tag{89}$$

$$\begin{cases}0<m_{\omega.e}<\dfrac{2\omega L_e}{T_{c.\omega}V_A^2}\\ 0<n_{v.e}<\dfrac{2\omega L_e}{V_A}.\end{cases}\tag{90}$$

According to (88), the convergent limits of $\theta_{a.k}$ and $V_{a.k}$ can obtained as given in (91). This equation proves that the phase and effective value of $\vec{V}_{o.a}$ will be equal to $\vec{V}_m$ after a certain length of time. It means the initial phase difference and amplitude difference between $\vec{V}_{o.a}$ and $\vec{V}_m$ will be eliminated by the proposed method

$$\begin{cases}\lim\limits_{k\to\infty}\theta_{a.k}=0\\ \lim\limits_{k\to\infty}V_{a.k}=V_A.\end{cases}\tag{91}$$

The convergence limit of $P_{\text{cir}.a}$ and $Q_{\text{cir}.a}$ can be obtained by substituting (91) into (86), as given in (92). It proves that the proposed $\omega-P_{\text{cir}}$ and $V-Q_{\text{cir}}$ control can eliminate the active and reactive CCP simultaneously. Moreover, the performance of power sharing will not be influenced by the wire impedance

$$\begin{cases}\lim\limits_{k\to\infty}P_{\text{cir}.a.k}=\lim\limits_{k\to\infty}\dfrac{k_aV_A^2}{\omega L_e}\cdot\theta_{a.k}=0\\ \lim\limits_{k\to\infty}Q_{\text{cir}.a.k}=\lim\limits_{k\to\infty}\dfrac{k_aV_A}{\omega L_e}\cdot(V_{a.k}-V_A)=0.\end{cases}\tag{92}$$

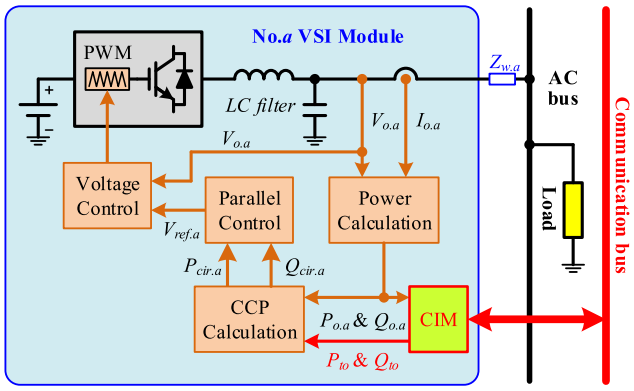

Fig. 7. System diagram of the proposed control method.

Moreover, according to the characteristic of convergent sequence, the convergent rate is the fastest when the relationship of (93) is complied with. In this condition, the droop coefficients $m_{\omega.e}$ and $n_{v.e}$ are defined as $m_{T.e}$ and $n_{T.e}$, respectively, which can be expressed as (94). It means, the proposed control method can realize the accurate active- and reactive-power sharing in the shortest time when $m_{\omega.e}$ and $n_{v.e}$ are equal to $m_{T.e}$ and $n_{T.e}$, and this time is only one control cycle theoretically. Therefore, $m_{T.e}$ and $n_{T.e}$ are defined as the optimum value of equivalent droop coefficients

$$\begin{cases} 1 - \dfrac{m_{\omega.e} T_{c.\omega} V_A^2}{\omega L_e} = 0 \\ 1 - \dfrac{n_{v.e} V_A}{\omega L_e} = 0 \end{cases} \tag{93}$$

$$\begin{cases} m_{T.e} = \dfrac{\omega L_e}{T_{c.\omega} V_A^2} \\ n_{T.e} = \dfrac{\omega L_e}{V_A}. \end{cases} \tag{94}$$

D. Implementation of the Proposed Method

Comparing with the droop method, the realization of the proposed method is more complicated due to the calculation of $P_{\text{cir}.a}$ and $Q_{\text{cir}.a}$. This calculation needs the data of all VSIs' output power as given in (67), thus the communication among the VSIs is unavoidable for the proposed method. Apparently, the communication will sharply reduce the reliability and expansibility comparing with the traditional droop method.

The proposed method can be implemented by several structures with communications, such as centralized control, master–slave control, and distributed control. Comparing to the other two structures, the distributed control has better reliability and redundancy, and it is adopted as the control system of the simulation platform and experiment prototype system in this paper.

Fig. 7 shows the system diagram of the proposed method. In this system, every VSI calculates its own $P_{o.a}$ and $Q_{o.a}$ by the power calculation module. The communication interface module transmits $P_{o.a}$ and $Q_{o.a}$ to other VSIs and receives the power information of other VSIs by the communication bus. Subsequently, $P_{\text{cir}.a}$ and $Q_{\text{cir}.a}$ is calculated by the CCP calculation module. The parallel-operation control module will execute the control equation of (84), and generate the reference voltage $V_{\text{ref}.a}$. Finally, the voltage control module will control and adjust the output voltage $V_{o.a}$ by following $V_{\text{ref}.a}$.

In this diagram, $P_{o.a}$ and $Q_{o.a}$ transmitted by communication are not the instantaneous power but the average power, so it is a low-frequency communication as low as the power frequency, which can reduce the cost of communication and improve the system reliability. Moreover, when the communication breaks down, the control strategy will transfer from the proposed method to the droop method, which can greatly improve the system stability and reliability.

Moreover, the communication also can transmit additional information in order to realize additional functions. For example, [38] proposed a control method in the microgird application, in which the bias power information is transmitted to every VSI module from a central control center in order to adjust the amplitude and frequency of the steady-state voltage of VSIPS, and it can realize the synchronization of ac bus voltage and grid voltage before the operation mode of microgrid transfers from the islanding mode to the grid-tied mode.

TABLE I
WIRE IMPEDANCE OF VSI MODULES

	No. 1	No. 2	No. 3	No. 4	No. 5
Wire inductance (μH)	100	200	300	400	500
Wire resistance (mΩ)	0.1	0.2	0.3	0.4	0.5
Weight coefficient k_a	60/137	30/137	20/137	15/137	12/137

VII. VERIFICATION OF THE PROPOSED MATHEMATICAL MODELS

A simulation system consisting of five VSI modules is established by the simulation software PLECS in order to verify the VSIPS mathematical model and CCPPM. In this system, VSI modules are simulated by the ideal voltage sources, and the system diagram is the same as Fig. 1. And the simulation results are presented as follows.

A. Verification of the VSIPS Mathematical Model

In order to verify the VSIPS mathematical model, the voltages of VSIs are designed to equal to V_m, of which the effective value is 110 V, frequency is 50 Hz, and the phase angle is 0, which complies with the definition of the steady state of VSIPS. The wire impedance of VSIs are listed in Table I, and VSIs' weighted coefficient k_a can be calculated according to the wire impedance, which are also listed in Table I. According to the mathematical model of VSIPS, the output current of every VSI should comply with the relationship of (9), and the circulating current of VSIs should be zero.

Fig. 8 shows the waveforms of $I_{o.a}$ and $I_{\text{cir}.a}$ in the simulation when Z_{load} is 3 Ω. According to simulation results, the effective value of I_{load} is 54.9963 A, and the effective values of $I_{o.a}$ are 24.0860, 12.0430, 8.0287, 6.0215 and 4.8172 A, respectively.

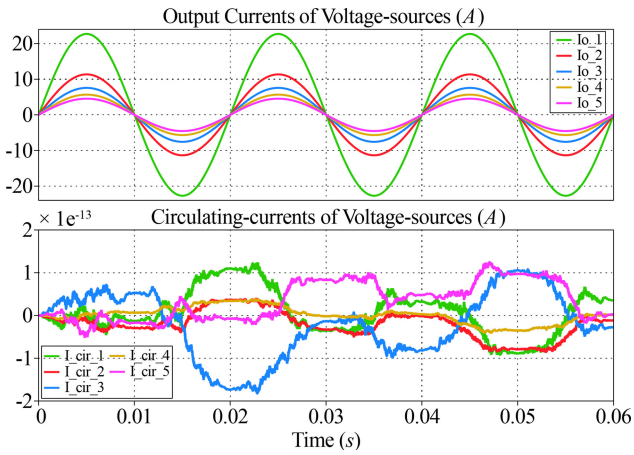

Fig. 8. Simulation results of a steady-state model.

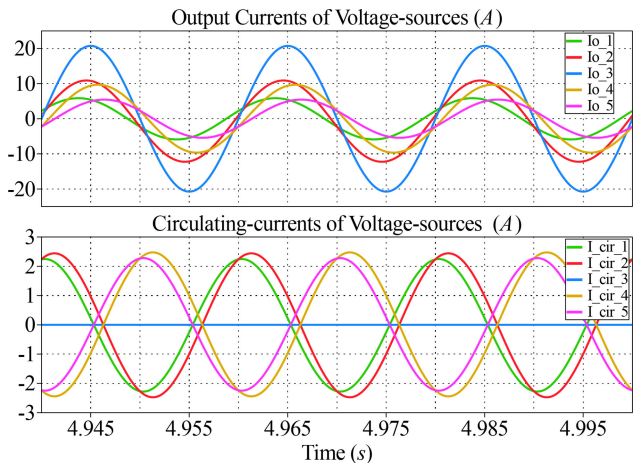

Fig. 9. Simulation results of a small-signal model.

TABLE II
SIMUALTION PARAMETERS

	No. 1	No. 2	No. 3	No. 4	No. 5
Effective value of voltage (V)	109.9	109.95	110	110.05	110.1
Phase of voltage (rad)	1×10^{-4}	2×10^{-4}	0	-2×10^{-4}	-1×10^{-4}
Wire inductance (μH)	200	100	50	100	200
Wire resistance (mΩ)	0.2	0.1	0.05	0.1	0.2
Weight coefficient k_a	0.1	0.2	0.3	0.2	0.1

TABLE III
THEORETICAL VALUES OF $P_{\text{CIR}.a}$ AND $Q_{\text{CIR}.a}$

	No. 1	No. 2	No. 3	No. 4	No. 5
$P_{\text{cir}.a}$ (W)	18.700	76.473	0.000	–76.473	–18.700
$Q_{\text{cir}.a}$ (Var)	–175.007	–174.823	0.000	174.823	175.007

TABLE IV
SIMULATION RESULTS OF $P_{\text{CIR}.a}$ (W)

R_{load} (Ω)	No. 1	No. 2	No. 3	No. 4	No. 5
1	17.584	75.329	0.041	–75.358	–17.597
3	18.318	76.065	0.041	–76.093	–18.331
12	18.593	76.34	0.041	–76.368	–18.606

TABLE V
SIMULATION RESULTS OF $Q_{\text{CIR}.a}$ (Var)

R_{load} (Ω)	No. 1	No. 2	No. 3	No. 4	No. 5
1	–174.8	–174.8	–0.198	174.77	175.07
3	–174.9	–175.1	–0.198	175.09	175.14
12	–175	–175.2	–0.198	175.21	175.17

As the data present, the simulation results of $I_{o.a}$ and I_{load} comply with the relationship of (9), which proves the proposed steady-state model of VSIPS. Meanwhile, the effective value of $I_{\text{cir}.a}$ is smaller than 2×10^{-13}A, so $I_{\text{cir}.a}$ is an infinitesimal comparing to $I_{o.a}$, which verifies the proposed circulating-current small-signal model of VSIPS. Moreover, the same conclusions can be obtained when Z_{load} is set as other values.

B. Verification of CCPPM

In order to verify the CCPPM, the effective value, frequency, and phase of $\vec{V}_m$ is assumed as 110 V, 50 Hz, and 0, and the parameters of VSIs' voltages are listed in Table II, which comply with the relationship of (34). According to CCPPM, the theoretical value of $P_{\text{cir}.a}$ and $Q_{\text{cir}.a}$ can be calculated by (64), which are listed as shown in Table III.

Fig. 9 shows the simulation waveforms of $I_{o.a}$ and $I_{\text{cir}.a}$ when Z_{load} is 3 Ω. This figure shows the circulating currents among VSIs are obvious, which are caused by the voltage difference. Meanwhile, $P_{\text{cir}.a}$ and $Q_{\text{cir}.a}$ can be calculated according to the simulation results of $P_{o.a}$ and $Q_{o.a}$ by (67), and their values at different loads are listed in Tables IV and V.

Comparing Tables IV and V with Table III, the simulating result of CCP is close to the theoretical result, which can prove the accuracy of CCPPM. Meanwhile, these tables show that simulation results of $P_{\text{cir}.a}$ and $Q_{\text{cir}.a}$ are influenced by Z_{load}. The smaller the Z_{load}, the larger the error of simulation result. Therefore, it proved that the equivalent wire impedance of VSIPS should be far less than Z_{load} in order to reduce the influence of Z_{load} on the calculation of P_{cir} and Q_{cir}.

VIII. VERIFICATION OF THE PROPOSED CONTROL METHOD

A. Implementation of the Prototype System of VSIPS

A VSIPS prototype system consisting of three 3-kVA VSI modules with 110 V/50 Hz voltage is established, in order to verify the performance of the proposed control method. Fig. 10 shows the picture of the prototype system, and the system structure can be shown as Fig. 11. As these figures show, every VSI module is connected to the ac bus by the wire impedance, and the communication of VSI modules is realized by controller area network (CAN) bus.

The VSI modules are designed based on the power stages of 3-kVA single-phase inverter from *Technology Dynamics Inc.*

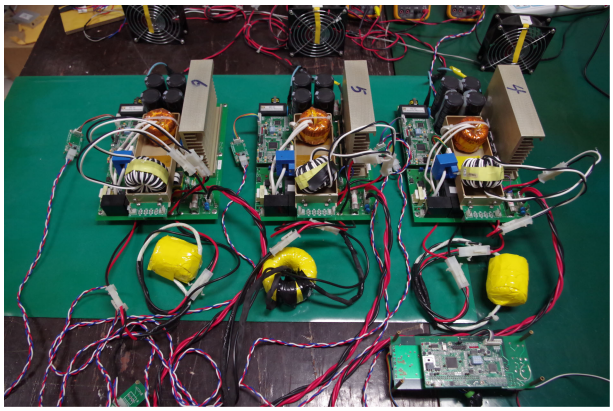

Fig. 10. VSIPS prototype system (9 kVA/110 V/50 Hz).

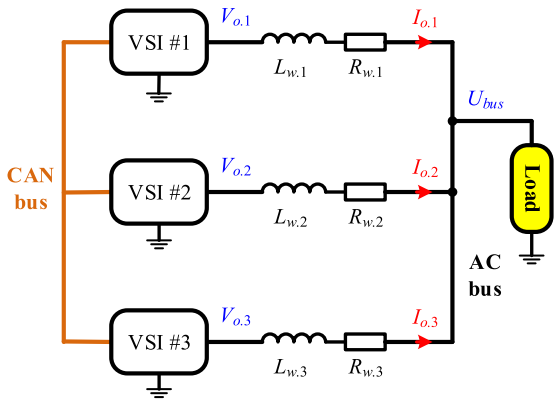

Fig. 11. Structure of VSIPS prototype system.

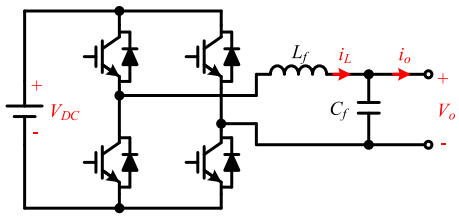

Fig. 12. Topology of the power circuit of VSI modules.

The topology of power circuit of VSI modules can be shown as Fig. 12, which consisted of a single-phase IGBT full-bridge and a *LC* output filter. The controller of VSI modules was implemented by DSP of TMS320F2808 (32-bit fixed-point 100 MHz) from *Texas Instruments*. The parameters of VSI modules are listed in Table VI.

Fig. 13 shows the diagram of the traditional double-loop output voltage control, which consists of the outer loop control of instantaneous output voltage and the inner loop control of instantaneous filter-inductor current. This control is adopted by every VSI module in order to track the reference voltage V_{ref}, which is generated by the parallel-operation control. Moreover, the design of the voltage control should ensure every VSI module perform as a robust voltage source, in order to reduce the impact of VSIs' internal impedance on the parallel operation of VSI modules.

TABLE VI
PARAMETERS OF VSI MODULES

Parameters	*Value*	*Unit*
Rated output power (S_{RA})	3	kVA
Effective value of rated output voltage (V_A)	110	V
Frequency of rated output voltage (f_o)	50	Hz
Switching frequency (f_s)	20	kHz
Analog/Digital (AD) Sampling frequency (f_{AD})	20	kHz
Inductance of output filter (L_f)	600	μH
Capacitance of output filter (C_f)	20	μF

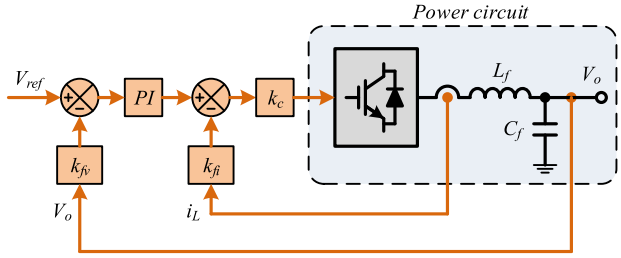

Fig. 13. Diagram of double-loop control of output voltage.

In this system, the wire impedance of every VSI is designed as a pure inductive ($L_{w.a}$) based on the analysis of this paper, which is realized by an inductor that connects every VSI to the ac bus. But the parasitic components of wire impedance still exist in this system, which will have the influence on the power sharing in VSIPS.

So according to (37) and (62), the range of $L_{w.a}$ can be expressed as (95). After substituting the values given in Table VI into (95), the result can be obtained that $L_{w.a}$ should be no larger than 257 μH. Therefore, the theoretical value of $L_{w.a}$ is designed as 250 μH when $S_{\text{RA}.a}$ is 3 kVA in this system

$$L_{w.a} \le \frac{V_A^2}{100 \cdot \pi f_o S_{\text{RA}.a}}. \tag{95}$$

Subsequently, the optimum droop coefficients $m_{T.a}$ and $n_{T.a}$ of $\omega - P_{\text{cir}}$ and $V - Q_{\text{cir}}$ control can be calculated by (96), which is obtained based on (69) and (94)

$$\begin{cases} m_{T.a} = \dfrac{m_{T.e}}{k_a} = \dfrac{\omega L_{w.a}}{T_{c.\omega} V_A^2} \\ n_{T.a} = \dfrac{n_{T.e}}{k_a} = \dfrac{\omega L_{w.a}}{V_A}. \end{cases} \tag{96}$$

Moreover, the control system of VSIs uses the power calculation method proposed in [15]. According to the analysis in [15], $T_{c.\omega}$ in (96) should not be less than the active-power calculation period in order to guarantee $\theta_{a.k}$ convergent, which is one quarter of the power-line period, so $T_{c.\omega}$ is designed as 5 ms in the prototype system. Thus, the values of $m_{T.a}$ and $n_{T.a}$ can be obtained based on Table VI, which are 6.488×10^{-4} and 7.136×10^{-4}, and their units are rad/W·s and V/Var, respectively.

The comparison simulation and experiment of traditional droop control and the proposed control are performed based on the above-mentioned design, and the results are expressed as

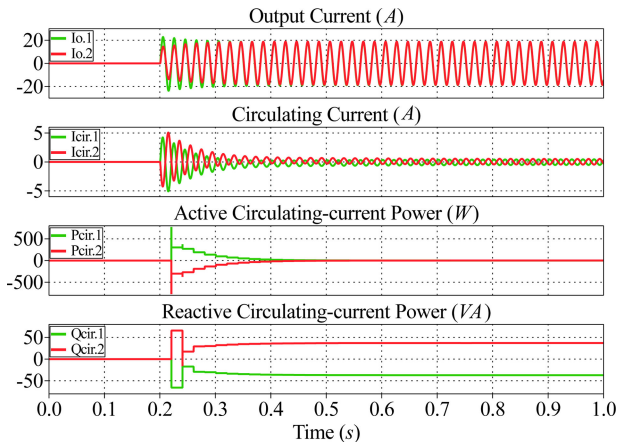

Fig. 14. Simulation results of the droop method.

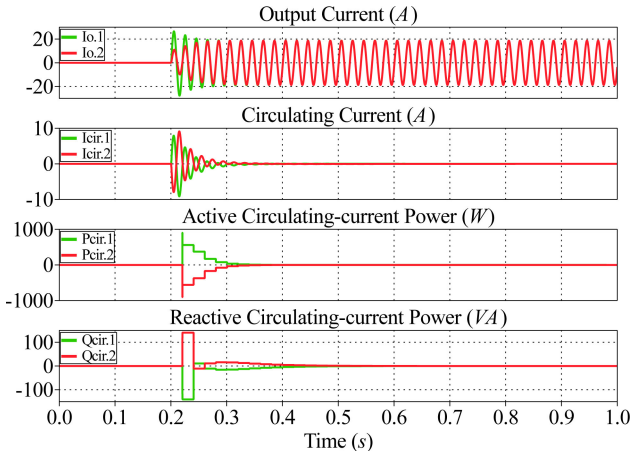

Fig. 15. Simulation results of the proposed method.

follows. For a fair comparison, both the methods use the same droop coefficients, the same power calculation method, and the same voltage-source control strategy, and are tested on the same prototype system at the same load conditions.

B. Simulation Results

A simulation system consisting of two 3-kVA VSIs is established by PLECS, based on the design of Section VIII-A. The initial effective values of two VSIs are set as 109.8 and 110.2 V, and the initial phase difference between two VSIs is set as 0.0314 rad.

Figs. 14 and 15 show the simulation results of the droop method and the proposed method, respectively, when Z_{load} is a 4.1-Ω resistor. Comparing the waveforms in the steady state, there are obvious circulating currents in Fig. 14, and the circulating currents in Fig. 15 are sharply reduced. Moreover, as shown in Fig. 14, P_{cir} of two VSIs equals 0 approximately, and Q_{cir} is about 37 and –37 Var in the steady state. Whereas in Fig. 15, both P_{cir} and Q_{cir} are equal to 0 approximately in the steady state.

Therefore, the simulation results verify that the traditional droop control cannot realize accurate reactive-power sharing,

TABLE VII
PARAMETERS OF VSIPS IN 1:1:1 SHARING RATIO

Parameters	Module 1	Module 2	Module 3
Inductive impedance $L_{w.a}$ (μH)	242.7	243.6	243.0
Resistive impedance $R_{w.a}$ (Ω)	0.057	0.071	0.061
Droop coefficient $m_{\omega.a}$ (rad/W·s)	6.488×10^{-4}	6.488×10^{-4}	6.488×10^{-4}
Droop coefficient $n_{v.a}$ (V/Var)	7.136×10^{-4}	7.136×10^{-4}	7.136×10^{-4}

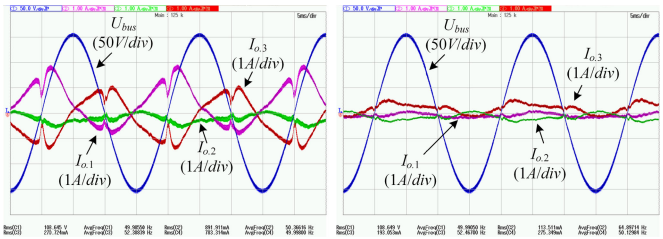

Fig. 16. Experiment results at the nonload (Sharing ratio is 1:1:1). (a) Droop method. (b) Proposed method.

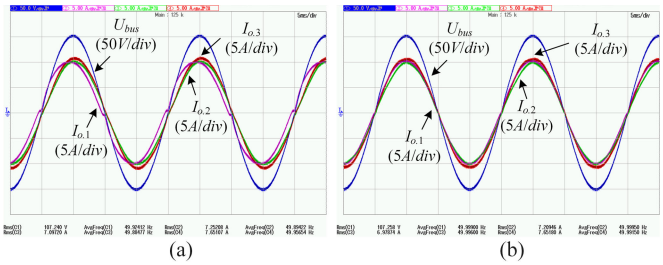

Fig. 17. Experiment results at 2300 VA linear load (Sharing ratio is 1:1:1). (a) Droop method. (b) Proposed method.

but the proposed method can realize the accurate active-power and reactive-power sharing simultaneously.

C. Experimental Results

The comparison experiment included two separate parts: the common loads are shared by VSIs equally and unequally.

1) When the Load Power is Shared Equally: In this experiment, the droop coefficients and the measured values of wire impedance of every VSI are given in Table VII. The values of $R_{w.a}$ in this table are mainly caused by the parasitic resistance of the wires.

Fig. 16 shows the waveforms of ac bus voltage U_{bus}, and output currents of VSIs ($I_{o.1}$, $I_{o.2}$, and $I_{o.3}$) at nonload in steady state, which are the results of the droop method and the proposed method, respectively. Similarly, Fig. 17 shows the waveforms at 2300 VA linear load, Fig. 18 shows the waveforms at 8700 VA linear load, Fig. 19 shows the waveforms at 1600 VA nonlinear load, and Fig. 20 shows the waveforms at 4800 VA nonlinear load.

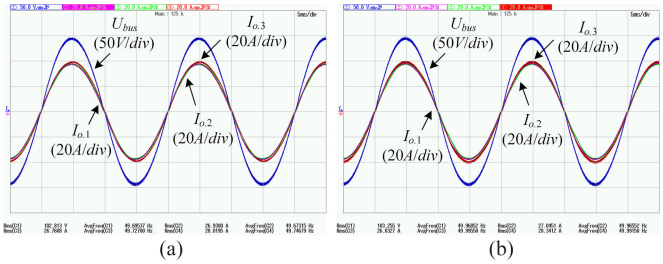

Fig. 18. Experiment results at 8700 VA linear load (Sharing ratio is 1:1:1). (a) Droop method. (b) Proposed method.

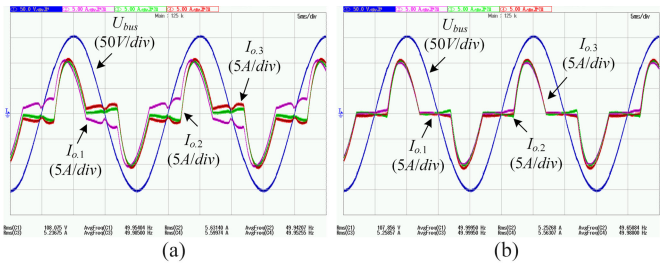

Fig. 19. Experiment results at 1600 VA nonlinear load (Sharing ratio is 1:1:1). (a) Droop method. (b) Proposed method.

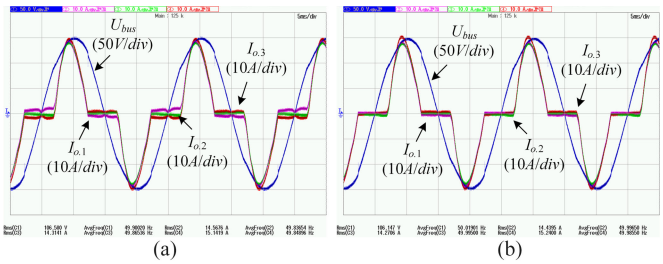

Fig. 20. Experiment results at 4800 VA nonlinear load (Sharing ratio is 1:1:1). (a) Droop method. (b) Proposed method.

According to the comparison of the experiments, the proposed method can sharply reduce the circulating current at nonload, nonlinear load, and light linear load, which is much better than the droop method, while the performance of the proposed method is similar as the droop method at heavy linear load.

Moreover, $P_{\text{cir.RMS}}$ and $Q_{\text{cir.RMS}}$ are defined in this paper in order to evaluate the CCP in VSIPS, which can be expressed by (97). Therefore, according to the values of $P_{\text{cir}.a}$ and $Q_{\text{cir}.a}$ calculated by DSP controllers of VSI modules, the comparison of $P_{\text{cir.RMS}}$ and $Q_{\text{cir.RMS}}$ between the droop method and the proposed method can be obtained, as shown in Figs. 21 and 22

$$\begin{cases} P_{\text{cir.RMS}} = \sqrt{\frac{1}{n}\sum_{j=1}^{n} P_{\text{cir}.j}^2} \\ Q_{\text{cir.RMS}} = \sqrt{\frac{1}{n}\sum_{j=1}^{n} Q_{\text{cir}.j}^2} \end{cases}. \tag{97}$$

As shown in Fig. 21, $P_{\text{cir.RMS}}$ in the droop method and the proposed method are both less than 5 W. Even at some loads, $P_{\text{cir.RMS}}$ in the proposed method are slightly more than the droop method. However, as shown in Fig. 22, $Q_{\text{cir.RMS}}$ in the droop method are between 20 and 114 Var, whereas all the values in the proposed method are less than 3.0 Var, which is far less than the droop method.

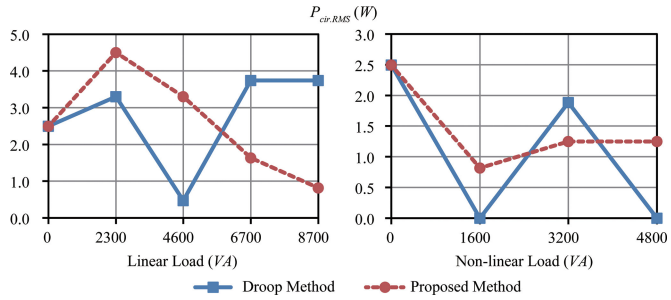

Fig. 21. Comparison of $P_{\text{cir.RMS}}$ (Sharing ratio is 1:1:1).

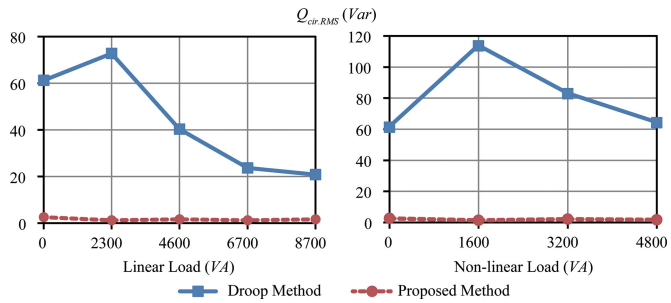

Fig. 22. Comparison of $Q_{\text{cir.RMS}}$ (Sharing ratio is 1:1:1).

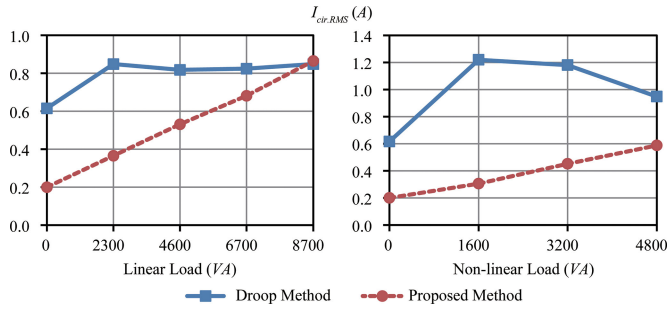

Fig. 23. Comparison of $I_{\text{cir.RMS}}$ (Sharing ratio is 1:1:1).

Meanwhile, the circulating current $I_{\text{cir.RMS}}$ is defined in this paper in order to evaluate the circulating current in VSIPS, as given in (98). In this equation, $I_{\text{cir}.a.\text{RMS}}$ is the effective value of every VSI's circulating current $I_{\text{cir}.a}$, and its value is calculated by the software of Yokogawa based on the measured results of Yokogawa oscilloscope (DLM2024)

$$I_{\text{cir.RMS}} = \sqrt{\frac{1}{n}\sum_{j=1}^{n} I_{\text{cir}.j.\text{RMS}}^2}. \tag{98}$$

So the comparison of $I_{\text{cir.RMS}}$ between the droop method and the proposed method is shown Fig. 23. As this figure shows that $I_{\text{cir.RMS}}$ in the proposed method and droop method are similar at heavy linear load, whereas at nonload, nonlinear load, and light linear load, $I_{\text{cir.RMS}}$ in the proposed method is much less than the droop method, which proves that the power-sharing performance of the proposed method is much better than the droop method.

2) When the Load Power is Shared Unequally: In this experiment, the load power is shared by three VSI modules based on the sharing ratio of 2:1:2, and the rated output power of the second VSI module is set as 1.5 kVA, so the theoretical value of

TABLE VIII
PARAMETERS OF VSIPS IN 2:1:2 SHARING RATIO

Parameters	Module 1	Module 2	Module 3
Inductive impedance $L_{w.a}$ (μH)	242.7	485.0	243.0
Resistive impedance $R_{w.a}$ (Ω)	0.057	0.071	0.061
Droop coefficient $m_{\omega.a}$ (rad/W·s)	6.488×10^{-4}	1.298×10^{-3}	6.488×10^{-4}
Droop coefficient $n_{v.a}$ (V/Var)	7.136×10^{-4}	1.427×10^{-3}	7.136×10^{-4}

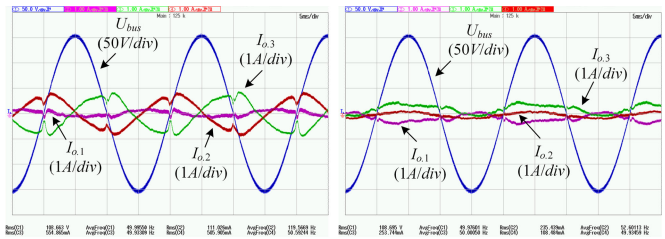

Fig. 24. Experiment results at the nonload (Sharing ratio is 2:1:2). (a) Droop method. (b) Proposed method.

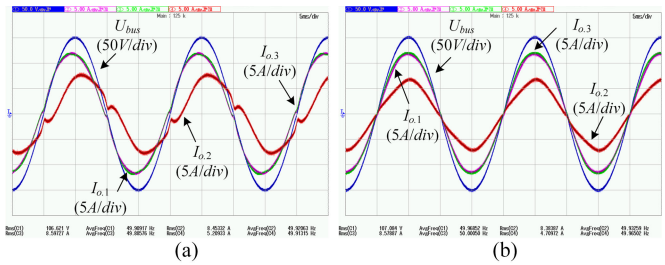

Fig. 25. Experiment results at 2300 VA linear load (Sharing ratio is 2:1:2). (a) Droop method. (b) Proposed method.

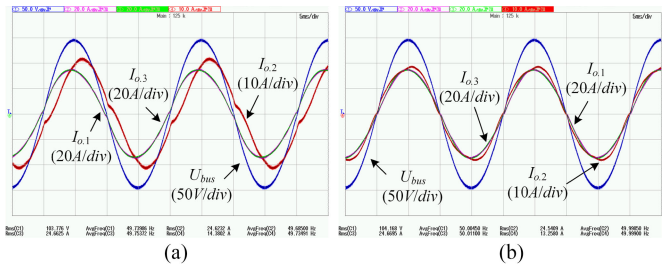

Fig. 26. Experiment results at 8700 VA linear load (Sharing ratio is 2:1:2). (a) Droop method. (b) Proposed method.

wire inductance $L_{w.2}$ is designed as 500 μH according to (95). Meanwhile, the droop coefficients and the measured values of wire impedance are given in Table VIII.

Fig. 24 shows the waveforms of U_{bus}, $I_{o.1}$, $I_{o.2}$, and $I_{o.3}$ at nonload in steady state, which are the results of the droop method and the proposed method, respectively. Similarly, Fig. 25 shows the waveforms at 2300 VA linear load, Fig. 26 shows the waveforms at 6700 VA linear load, Fig. 27 shows the waveforms at 1600 VA nonlinear load, and Fig. 28 shows the waveforms at 4800 VA nonlinear load.

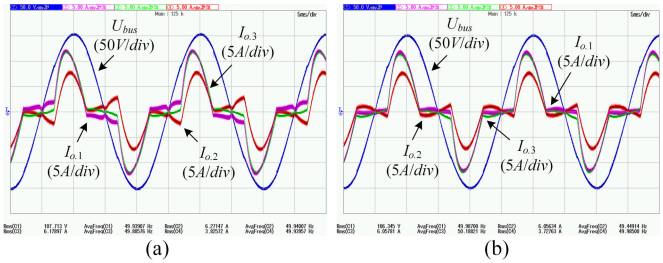

Fig. 27. Experiment results at 1600 VA nonlinear load (Sharing ratio is 2:1:2). (a) Droop method. (b) Proposed method.

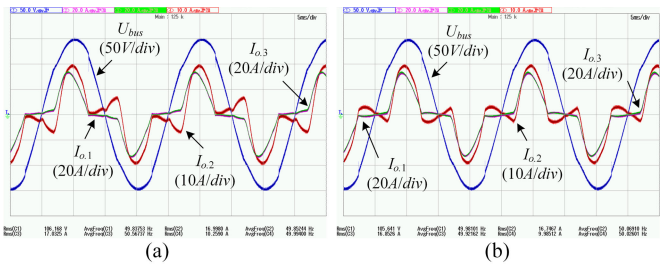

Fig. 28. Experiment results at 4800 VA nonlinear load (Sharing ratio is 2:1:2). (a) Droop method. (b) Proposed method.

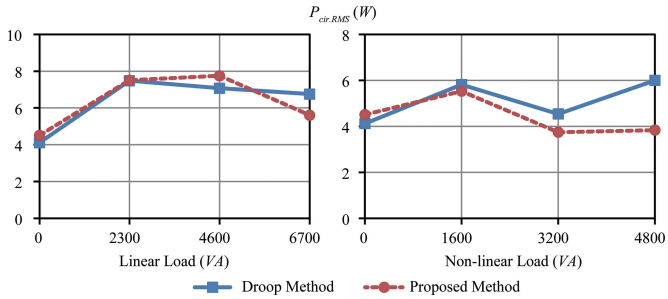

Fig. 29. Comparison of $P_{\text{cir.RMS}}$ (Sharing ratio is 2:1:2).

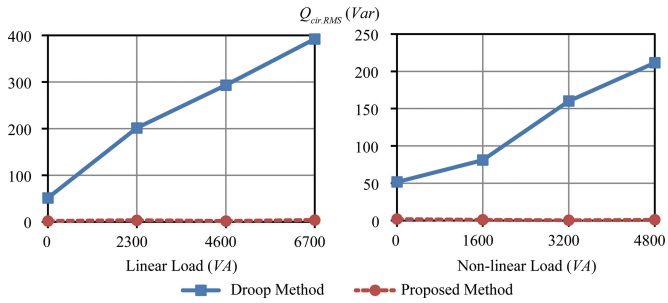

Fig. 30. Comparison of $Q_{\text{cir.RMS}}$ (Sharing ratio is 2:1:2).

According to the results of the comparison of the experiments, the proposed method can sharply reduce the circulating current at any load, which is much better than the droop method.

Figs. 29 and 30 show the comparison of $P_{\text{cir.RMS}}$ and $Q_{\text{cir.RMS}}$ between the droop method and the proposed method. As shown in Fig. 29, $P_{\text{cir.RMS}}$ in the two methods is less than 8 W. However, as shown in Fig. 30, $Q_{\text{cir.RMS}}$ in droop method is between 50 and 400 Var, and most of the values are more than 100 Var, whereas all the values in the proposed method are less than 4.5 Var, and

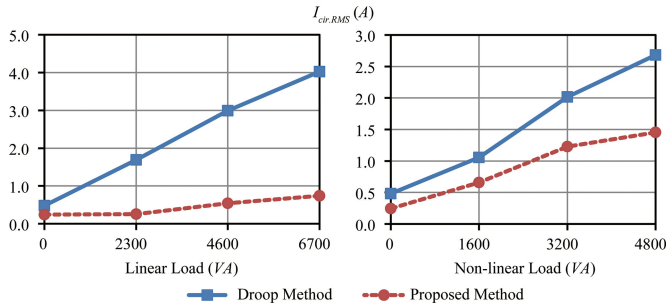

Fig. 31. Comparison of $I_{\mathrm{cir.RMS}}$ (Sharing ratio is 2:1:2).

most of the values are less than 2.5 Var, which is far less than the droop method.

Fig. 31 shows the comparison of $I_{\mathrm{cir.RMS}}$ between the droop method and the proposed method. As this figure shows, $I_{\mathrm{cir.RMS}}$ in the proposed method is obviously smaller than the droop method at any load, which verifies that the power-sharing performance of the proposed method is much better than the droop method.

D. Summary

Conclusions can be obtained by the simulation and experiment comparison between the traditional droop method and the proposed method in this section:

1) the performance of the proposed method on restraining I_{cir} is better than the droop method;
2) the droop method and the proposed method have the same performance on restraining P_{cir};
3) the performance of the proposed method on restraining Q_{cir} is much better than the droop method;
4) even though the proposed method does not have the special control for the harmonic circulating current, it still has better power-sharing performance than the droop control at the nonlinear load;
5) although it is designed on the pure inductive wire impedance in theory, the proposed method shows good power-sharing performance on the complex wire impedance in the experiment.

Therefore, the proposed method can efficiently inhibit circulating currents and decrease both the active and reactive CCP, which verifies that it has better power-sharing performance comparing to the traditional droop control.

IX. Conclusion

This paper proposes an optimized mathematical model of VSIPS and proposes an improved droop control method based on this model, which can realize accurate power sharing in VSIPS. The major work of this paper includes three parts: the system modeling and analysis of VSIPS, the modeling analysis of traditional droop control, and the design of the accurate power-sharing control method. And all these parts are validated by the simulation and experimental results presented in this paper.

Comparing to the traditional droop control, the proposed method has much better performance of active-and reactive-power sharing, especially when the load is shared unequally. However, the implementation of the proposed method needs the communication between VSIs, which will reduce the reliability and expansibility of VSIPS, and this is a challenge for the application of the proposed method in the future work. Moreover, the proposed method does not have the special control for the harmonic circulating current and the uncontrollable parasitic impedance, and the analysis and design of the harmonic-current control and wire-impedance control will be the future research of this paper.

Acknowledgment

The authors would like to thank Technology Dynamics Inc., for the support of the single-phase inverter power stage during the project. They would like to thank PLEXIM Inc., for the support of the powerful simulation tools PLECS.

References

[1] F. Z. Peng, Y. W. Li, and L. M. Tolbert, "Control and protection of power electronics interfaced distributed generation systems in a customer-driven microgrid," in *Proc. IEEE Power Energy Soc. Gen. Meet.*, Calgary, AB, Canada, 2009, pp. 1−8.

[2] J. M. Guerrero, L. G. de Vicuna, J. Matas, M. Castilla, and J. Miret, "Output impedance design of parallel-connected UPS inverters with wireless load-sharing control," *IEEE Trans. Ind. Electron.*, vol. 52, no. 4, pp. 1126–1135, Aug. 2005.

[3] J. M. Guerrero, J. Matas, L.G. de Vicuna, M. Castilla, and J. Miret, "Wireless-control strategy for parallel operation of distributed-generation inverters," *IEEE Trans. Ind. Electron.*, vol. 53, no. 5, pp. 1461–1470, Oct. 2006.

[4] J. M. Guerrero, J. Matas, L. G. de Vicuna, M. Castilla, and J. Miret, "Decentralized control for parallel operation of distributed generation inverters using resistive output impedance," *IEEE Trans. Ind. Electron.*, vol. 54, no. 2, pp. 994–1004, Apr. 2007.

[5] K. De Brabandere, B. Bolsens, J. Van den Keybus, A. Woyte, J. Driesen and R. Belmans, "A voltage and frequency droop control method for parallel inverters," *IEEE Trans. Power Electron.*, vol. 22, no. 4, pp. 1107–1115, Jul. 2007.

[6] H. Xu, X. Zhang, F. Liu, R. Shi, C. Yu, and R. Cao, "A reactive power sharing strategy of VSG based on virtual capacitor algorithm," *IEEE Trans. Ind. Electron.*, to be published.

[7] J. Matas, M. Castilla, L. G. de. Vicuña, J. Miret, and J. C. Vasquez, "Virtual impedance loop for droop-controlled single-phase parallel inverters using a second-order general-integrator scheme," *IEEE Trans. Power Electron.*, vol. 25, no. 12, pp. 2993–3002, Dec. 2010.

[8] S. Xu, J. Wang, and J. Xu, "A current decoupling parallel control strategy of single-phase inverter with voltage and current dual closed-loop feedback," *IEEE Trans. Ind. Electron.*, vol. 60, no. 4, pp. 1306–1313, Apr. 2013.

[9] X. Lyu, Y. Li, and D. Cao, "DC-Link RMS current reduction by increasing paralleled three-phase inverter module number for segmented traction drive," *IEEE J. Emerg. Sel. Topics Power Electron.*, vol. 5, no. 1, pp. 171–181, Mar. 2017.

[10] Y. Li and Y. W. Li, "Power management of inverter interfaced autonomous microgrid based on virtual frequency-voltage frame," *IEEE Trans. Smart Grid*, vol. 2, no. 1, pp. 30–22, Mar. 2011.

[11] Y. W. Li and C. N. Kao, "An accurate power control strategy for power-electronics-interfaced distributed generation units operating in a low-voltage multibus microgrid," *IEEE Trans. Power Electron.*, vol. 24, no. 12, pp. 2977–2988, Dec. 2009.

[12] W. Yao, M. Chen, J. Matas, J. M. Guerrero, and Z. M. Qian, "Design and analysis of the droop control method for parallel inverters considering the impact of the complex impedance on the power sharing," *IEEE Trans. Ind. Electron.*, vol. 58, no. 2, pp. 576–588, Feb. 2011.

[13] B. Liu, S. Zheng, Y. Ma, F. Wang, and L. M. Tolbert, "Control and implementation of converter based ac transmission line emulation," in *Proc. IEEE Appl. Power Electron. Conf. Expo.*, Mar. 2015, pp. 1807–1814.

[14] J. M. Guerrero, L. G. de Vicuna, J. Matas, M. Castilla, and J. Miret, "A wireless controller to enhance dynamic performance of parallel inverters in distributed generation systems," *IEEE Trans. Power Electron.*, vol. 19, no. 5, pp. 1205–1213, Sep. 2004.

[15] M. Gao, M. Chen, C. Jin, J. M. Guerrero, and Z. Qian, "Analysis, design and experimental evaluation of power calculation in digital droop-controlled parallel microgrid inverters," *J. Zhejiang Univ. SCIENCE C (Comput. Electron.)*, vol. 14, no. 1, pp. 50−64, Jan. 2013.
[16] M. N. Marwali, J.-W. Jung, and A. Keyhani, "Control of distributed generation systems—Part II: Load sharing control," *IEEE Trans. Power Electron.*, vol. 19, no. 6, pp. 1551−1561, Nov. 2004.
[17] T. L. Lee and P. T. Cheng, "Design of a new cooperative harmonic filtering strategy for distributed generation interface converters in an islanding network," *IEEE Trans. Power Electron.*, vol. 22, no. 5, pp. 1919−1927, Sep. 2007.
[18] E. Rokrok and M. E. H. Golshan, "Adaptive voltage droop scheme for voltage source converters in an islanded multibus microgrid," *IET Gener. Transmiss. Distrib.*, vol. 4, no. 5, pp. 562–578, May 2010.
[19] Y. A. R. I. Mohamed and E. F. El-Saadany, "Adaptive decentralized droop controller to preserve power sharing stability of paralleled inverters in distributed generation microgrids," *IEEE Trans. Power Electron.*, vol. 23, no. 6, pp. 2806−2816, Nov. 2008.
[20] H. Bevrani and S. Shokoohi, "An intelligent droop control for simultaneous voltage and frequency regulation in islanded microgrids," *IEEE Trans. Smart Grid*, vol. 4, no. 3, pp. 1505−1513, Sep. 2013.
[21] C. T. Lee, C. C. Chu, and P. T. Cheng, "A new droop control method for the autonomous operation of distributed energy resource interface converters," *IEEE Trans. Power Electron.*, vol. 28, no. 4, pp. 1980–1993, Apr. 2013.
[22] X. Sun, B. Liu, Y. Cai, H. Zhang, Y. Zhu, and B. Wang, "Frequency-based power management for photovoltaic/battery/fuel cell-electrolyser standalone microgrid," *IET Power Electron.*, vol. 9, no. 13, pp. 2602–2610, Oct. 2016.
[23] X. Sun, Y. Hao, Q. Wu, X. Guo, and B. Wang, "A multifunctional and wireless droop control for distributed energy storage units in islanded AC microgrid applications," *IEEE Trans. Power Electron.*, vol. 32, no. 1, pp. 736–751, Jan. 2017.
[24] R. Majumder, B. Chaudhuri, A. Ghosh, R. Majumder, G. Ledwich, and F. Zare, "Improvement of stability and load sharing in an autonomous microgrid using supplementary droop control loop," *IEEE Trans. Power Syst.*, vol. 25, no. 2, pp. 796–808, May 2010.
[25] Y. Zhang and H. Ma, "Theoretical and experimental investigation of networked control for parallel operation of inverters," *IEEE Trans. Ind. Electron.*, vol. 59, no. 4, pp. 1961–1970, Apr. 2012.
[26] Y. Pei, G. Jiang, X. Yang, and Z. Wang, "Auto-master-slave control technique of parallel inverters in distributed ac power systems and UPS," in *Proc. IEEE 35th Annu. Power Electron. Spec. Conf.*, vol. 3, 2004, pp. 2050–2053.
[27] J. He and Y. W. Li, "An enhanced microgrid load demand sharing strategy," *IEEE Trans. Power Electron.*, vol. 27, no. 9, pp. 3984−3995, Sep. 2012.
[28] M. Gao, Y. Zhang, C. Jin, M. Chen, and Z. Qian, "An improved droop control method for parallel operation of distributed generations in microgrid," in *Proc. 28th Annu. IEEE Appl. Power Electron. Conf. Expo.*, Long Beach, CA, USA, 2013, pp. 3016–3020.
[29] H. Liang, B. J. Choi, W. Zhuang, and X. Shen, "Stability enhancement of decentralized inverter control through wireless communications in microgrids," *IEEE Trans. Smart Grid*, vol. 4, no. 1, pp. 321–331, Mar. 2013.
[30] Y. Zhang, M. Yu, F. Liu, and Y. Kang, "Instantaneous current-sharing control strategy for parallel operation of UPS modules using virtual impedance," *IEEE Trans. Power Electron.*, vol. 28, no. 1, pp. 432–440, Jan. 2013.
[31] J. M. Guerrero, M. Chandorkar, T. L. Lee, and P. C. Loh, "Advanced control architectures for intelligent microgrids—Part I: Decentralized and hierarchical control," *IEEE Trans. Ind. Electron.*, vol. 60, no. 4, pp. 1254–1262, Apr. 2013.
[32] J. M. Guerrero, J. C. Vasquez, J. Matas, L. G. de Vicuna, and M. Castilla, "Hierarchical control of droop-controlled ac and dc microgrids—A general approach toward standardization," *IEEE Trans. Ind. Electron.*, vol. 58, no. 1, pp. 158–172, Jan. 2011.
[33] J. C. Vasquez, J. M. Guerrero, M. Savaghebi, J. Eloy-Garcia, and R. Teodorescu, "Modeling, analysis, and design of stationary-reference-frame droop-controlled parallel three-phase voltage source inverters," *IEEE Trans. Ind. Electron.*, vol. 60, no. 4, pp. 1271–1280, Apr. 2013.
[34] J. M. Guerrero, J. C. Vasquez, J. Matas, L. G. de Vicuna, and M. Castilla, "Hierarchical control of droop-controlled ac and dc microgrids—A general approach toward standardization," *IEEE Trans. Ind. Electron.*, vol. 58, no. 1, pp. 158–172, Jan. 2011.
[35] J. W. He, Y. W. Li, J. M. Guerrero, J. C. Vasquez, and F. Blaabjerg, "An islanding microgrid reactive power sharing scheme enhanced by programmed virtual impedances," in *Proc. 3rd IEEE Int. Symp. Power Electron. Distrib. Gener. Syst.*, Aalborg, Denmark, 2012, pp. 229−235.
[36] F. Blaabjerg, Z. Chen and S. B. Kjaer, "Power electronics as efficient interface in dispersed power generation systems," *IEEE Trans. Power Electron.*, vol. 19, no. 5, pp. 1184–1194, Sep. 2004.
[37] R. Strzelecki, and G. Benysek, *Power Electronics in Smart Electrical Energy Networks*. London, U.K.: Springer, 2008.
[38] M. Gao, C. Zhang, M. Qiu, M. Chen, and A. Levy, "Design of control system for smooth mode transfer in smart microgrid application," in *Proc. IEEE Appl. Power Electron. Conf. Expo.*, Long Beach, CA, USA, 2016, pp. 138–142.

Mingzhi Gao (M'15) received the bachelor's degree in electronic and information engineering, in 2007, and the Ph.D. degree in electrical engineering, in 2014, from Zhejiang University, Hangzhou, China.

He is currently a Postdoctoral Researcher in power electronics and power driver at Zhejiang University, Hangzhou, China. His research interests include smart microgrid system, distributed power systems, wireless-parallel-inverter system, renewable energy systems, and digital control in power electronics.

Min Chen (M'09) received the B.S. degree in applied electronics and the Ph.D. degree in electrical engineering from Zhejiang University, Hangzhou, China, in 2000 and 2006, respectively.

From 2007 to 2009, he was a Postdoctoral Researcher in the Electrical Engineering Department, Zhejiang University, where he has been a Lecturer since 2010, and is currently an Associate Professor. From 2014 to 2015, he was a Visiting Researcher in the Department of Energy Technology, Aalborg University. Since 2007, he has been responsible for the Lighting Research and Development Laboratory, National Engineering Research Center for Applied Power Electronics. He has authored or coauthored more than 60 technical papers. He was issued for 14 patents of inventions. His research interests include power electronics in power system, inverter system, photovoltaic system and microinverter, electrical vehicle, regenerative energy system, distributed generation, energy storage system, modern lighting system for HID lamps and LED.

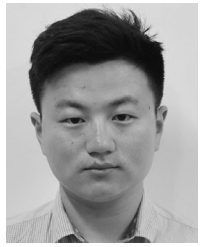

Chenxi Wang received the Bachelor's degree in electric engineering from the College of Electrical Engineering, Xi'an Jiaotong University, Xi'an, China, in 2015. He is currently working toward the Master's degree in power electronics and power driver at Zhejiang University, Hangzhou, China.

His research focuses on modular photovoltaic grid connected power generation technology and renewable energy systems.

Zhaoming Qian (SM'92) received the Graduate degree in radio engineering from the College of Electrical Engineering, Zhejiang University, Hangzhou, China, in 1961, and the Ph.D. degree in applied science from Catholic University of Leuven, Leuven, Belgium and the Interuniversity Microelectronics Center, Leuven, Belgium, in 1989.

Since 1961, he has been involved in teaching and the research on electronics and power electronics at Zhejiang University. In 1992, he was a Professor in the College of Electrical Engineering, Zhejiang University. He was the Deputy Director of National Engineering Research Center for Applied Power Electronics and the Deputy Director of Scientific Committee of National Key Laboratory of Power Electronics. He has authored or coauthored more than 200 papers published in international journals and conferences and one book on EMC design. His research interests include power electronics and its industrial applications, power electronic system integration, and electromagnetic compatibility in power electronic systems.

Dr. Qian has received the Excellent Education Awards from the China Education Commission and Zhejiang University in 1993, 1997, and 1999, respectively, and the Science and Technology Development Awards from the China Education Commission in 1999 and 2003, respectively.